15. Quark Model

Revised August 2021 by C. Amsler (Stefan Meyer Inst.), T. DeGrand (Colorado U., Boulder) and B. Krusche (Basel U.).

15.1 Introduction

Quantum chromodynamics (QCD) is the theory of strong interactions. QCD is a quantum field theory with an $SU(N_c)$ local "color" gauge symmetry with $N_c = 3$ colors and a collection of N_f "flavors" of colored fermions, the quarks. It involves a set of $N_c^2 - 1 = 8$ non-Abelian gauge fields, the gluons. QCD is believed to confine, that is, its physical states are color singlets with internal quark and gluon degrees of freedom. This review is concerned with the description of the properties (masses and matrix elements for couplings to electromagnetism and the weak intractions) of the low lying bound states of QCD. The shorthand expression for describing this physics is called the "quark model."

The spectrum of strongly interacting particles consists of a tower of many states, which can be either bosons (labelled as "mesons") or fermions (labelled as "baryons"). The spectrum of baryons and mesons exhibits a high degree of regularity. The organizational principle which best categorizes this regularity is encoded in the quark model. All descriptions of strongly interacting states use the language of the quark model. At the same time, the language is not precise. The quark model exists on many levels: at the simplest level, it is an almost dynamics-free picture of strongly interacting particles as bound states of quarks and antiquarks. As one refines the description, the quark model can become a a framework with more detailed descriptions of dynamics. At its most fundamental level, it might be a description of QCD.

At its heart, the quark model assumes that mesons are bound states of a quark - antiquark pair, and baryons are bound states of three quarks. These are the minimal particle content states which can be color singlets in an $SU(3)$ gauge theory. This approach cannot be justified directly from QCD; however, there is indirect evidence that this description has some fundamental validity from the version of QCD where the number of colors N_c is taken to infinity [1–3]. In that limit, mesons are dominantly narrow (width proportional to $1/N_c$) bound states of a quark - antiquark pair, and baryons have a mass which scales as N_c.

A better justification is that this approach works. Indeed, the quark model is much older (circa 1963-64) than QCD as a theory of the strong interactions (1973-1974). In fact, the principle issue in strong interaction physics before QCD was to justify the success of the quark model in systemizing the properties of mesons and baryons in terms of some more fundamental dynamics (QCD).

Today one knows that this is not the whole story. There are experimentally observed states which either cannot be described, or have an uncomfortable description, as minimal quark number states. Some of them have "exotic" (non- $\bar{q}q$ or qqq) quantum numbers. Given the successes of the quark model, these are classified as "tetraquarks, "pentaquarks" (or more) or "glueballs" (bound states of the gluonic degrees of freedom in QCD). Of course, such labels are imprecise: bound states with the same overall quantum numbers can mix, regardless of their internal degrees of freedom.

This review has several parts. We start by describing the properties of strongly interacting particles in terms of the properties of states made of a minimal number of quark fields which can be coupled into a color singlet – two fields (a quark and an antiquark) for the mesons, and three quarks, for a baryon. Quarks come in six flavors. We describe the properties of mesons as $\bar{q}q$ systems and baryons as qqq systems. Along the way we discuss hadronic bound states which do not fit into this classification.

Finally, at the end of this review, we present results from lattice simulations of QCD, a direct approach to the solution of QCD from its Lagrangian, without reference to models. Lattice simulations interact with the quark model in (at least) two ways: first, the interpolating fields which are used in lattice simulations are usually directly based on quark model constructions. That is the simplest way to create states with the desired quantum numbers, which can then be processed by the lattice calculation. The second way that lattice calculations interact with the quark model comes when one wishes to put the lattice calculations into some context: without the quark model, there are simply the results from the lattice calculations, and the results from experiment, and no way to understand why they are similar or different. The quark model is the framework which is almost universally used to generate that context. Of course, that statement is equally valid when one tries to systemize actual experimental data: the context is always some variation of a quark model.

15.2 Quantum numbers of the quarks

As gluons carry no intrinsic quantum numbers beyond color charge, and because color is believed to be permanently confined, the quantum numbers of strongly interacting particles are given by the quantum numbers of their constituent quarks and antiquarks.

Quarks are strongly interacting fermions with spin 1/2 and, by convention, positive parity. Antiquarks have negative parity. Quarks have the additive baryon number 1/3, antiquarks -1/3. Table 15.1 gives the other additive quantum numbers (flavors) for the three generations of quarks. They are related to the charge Q (in units of the elementary charge e) through the generalized Gell-Mann-Nishijima formula

$$\mathsf{Q} = \mathsf{I}_z + \frac{\mathcal{B} + \mathsf{S} + \mathsf{C} + \mathsf{B} + \mathsf{T}}{2} , \tag{15.1}$$

where $\mathcal{B}$ is the baryon number. The convention is that the quark *flavor* (I_z, S, C, B, or T) has the same sign as its *charge* Q. With this convention, any flavor carried by a charged meson has the same sign as its charge, *e.g.*, the strangeness of the K^+ is +1, the bottomness of the B^+ is +1, and the charm and strangeness of the D_s^- are each −1. Antiquarks have the opposite flavor signs. The hypercharge is defined as

$$\mathsf{Y} = \mathcal{B} + \mathsf{S} - \frac{\mathsf{C} - \mathsf{B} + \mathsf{T}}{3} .$$

Table 15.1: Quark quantum numbers.

	d	u	s	c	b	t
Q – electric charge	$-\frac{1}{3}$	$+\frac{2}{3}$	$-\frac{1}{3}$	$+\frac{2}{3}$	$-\frac{1}{3}$	$+\frac{2}{3}$
I – isospin	$\frac{1}{2}$	$\frac{1}{2}$	0	0	0	0
I_z – isospin z-component	$-\frac{1}{2}$	$+\frac{1}{2}$	0	0	0	0
S – strangeness	0	0	-1	0	0	0
C – charm	0	0	0	$+1$	0	0
B – bottomness	0	0	0	0	-1	0
T – topness	0	0	0	0	0	$+1$

Thus Y is equal to $\frac{1}{3}$ for the u and d quarks, $-\frac{2}{3}$ for the s quark, and 0 for all other quarks. More details and derivations on the quark structure of mesons and baryons can be found *e.g.* in Ref. [4].

15.3 Mesons

Mesons have baryon number $\mathcal{B} = 0$. In the quark model, they are $q\bar{q}'$ bound states of quarks q and antiquarks $\bar{q}'$ (the flavors of q and q' may be different). If the orbital angular momentum of the $q\bar{q}'$ state is ℓ, then the parity P is $(-1)^{\ell+1}$. The meson spin J is given by the usual relation $|\ell - s| \leq J \leq |\ell + s|$, where s is 0 (antiparallel quark spins) or 1 (parallel quark spins). The charge conjugation, or C-parity $C = (-1)^{\ell+s}$, is defined only for the $q\bar{q}$ states made of quarks and their own antiquarks. The C-parity can be generalized to the G-parity $G = (-1)^{I+\ell+s}$ for mesons made of quarks and their own antiquarks (isospin $\mathsf{I}_z = 0$), and for the charged $u\bar{d}$ and $d\bar{u}$ states (isospin $\mathsf{I} = 1$).

The mesons are classified in J^{PC} multiplets. The $\ell = 0$ states are the pseudoscalars (0^{-+}) and the vectors (1^{--}). The orbital excitations $\ell = 1$ are the scalars (0^{++}), the axial vectors (1^{++}) and (1^{+-}), and the tensors (2^{++}). Assignments for many of the known mesons are given in Tables 15.2, 15.3 and 15.4. Radial excitations are denoted by the principal quantum number n. The very short lifetime of the t quark makes it likely that bound-state hadrons containing t quarks and/or antiquarks do not exist.

States in the natural spin-parity series $P = (-1)^J$ must, according to the above, have $s = 1$ and hence, $CP = +1$. Thus, mesons with natural spin-parity and $CP = -1$ (0^{+-}, 1^{-+}, 2^{+-}, 3^{-+}, *etc.*) are forbidden in the $q\bar{q}'$ model. The $J^{PC} = 0^{--}$ state is forbidden as well. Mesons with such *exotic* quantum numbers may exist, but would lie outside the $q\bar{q}'$ model (see section 15.4 below on exotic mesons).

Following SU(3), the nine possible $q\bar{q}'$ combinations containing the light u, d, and s quarks are grouped into an octet and a singlet of light quark mesons:

$$\mathbf{3} \otimes \overline{\mathbf{3}} = \mathbf{8} \oplus \mathbf{1} \ . \tag{15.2}$$

A fourth quark such as charm c can be included by extending SU(3) to SU(4). However, SU(4) is badly broken owing to the much heavier c quark. Nevertheless, in an SU(4) classification, the sixteen mesons are grouped into a 15-plet and a singlet:

$$\mathbf{4} \otimes \overline{\mathbf{4}} = \mathbf{15} \oplus \mathbf{1} \ . \tag{15.3}$$

The *weight diagrams* for the ground-state pseudoscalar (0^{-+}) and vector (1^{--}) mesons are depicted in Fig. 15.1. The light quark mesons are members of nonets building the middle plane in Fig. 15.1(a) and (b).

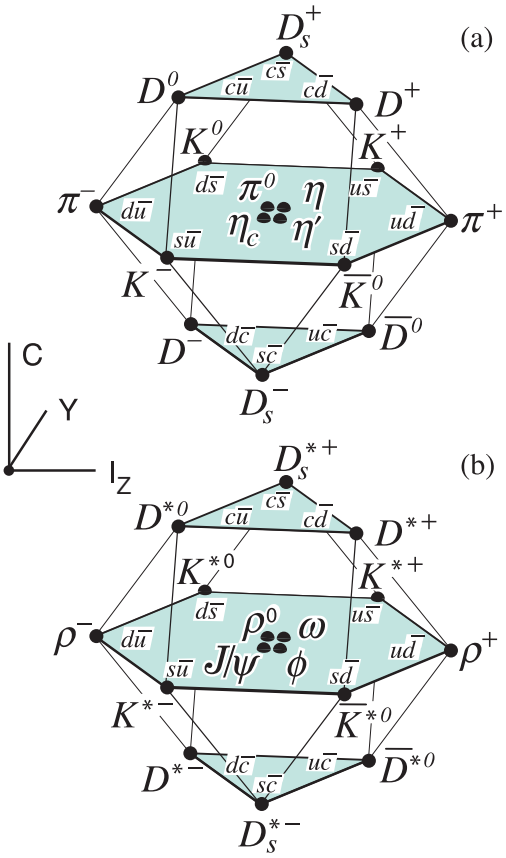

Figure 15.1: SU(4) weight diagram showing the 16-plets for the pseudoscalar (a) and vector mesons (b) made of the u, d, s, and c quarks as a function of isospin I_z, charm C, and hypercharge $\mathsf{Y} = \mathcal{B} + \mathsf{S} - \frac{\mathsf{C}}{3}$. The nonets of light mesons occupy the central planes to which the $c\bar{c}$ states have been added.

Isoscalar states with the same J^{PC} mix, but mixing between the two light quark isoscalar mesons, and the much heavier charmonium and bottomonium states, are generally assumed to be negligible. In the following, we shall use the generic names a for the $\mathsf{I} = 1$, K for the $\mathsf{I} = 1/2$, and f and f' for the $\mathsf{I} = 0$ members of the light quark nonets. Thus, the physical isoscalars are mixtures of the SU(3) wave function ψ_8 and ψ_1:

$$f' = \psi_8 \cos\theta - \psi_1 \sin\theta \ , \tag{15.4}$$

$$f = \psi_8 \sin\theta + \psi_1 \cos\theta \ , \tag{15.5}$$

where θ is the nonet mixing angle and

$$\psi_8 = \frac{1}{\sqrt{6}}(u\bar{u} + d\bar{d} - 2s\bar{s}) \ , \tag{15.6}$$

$$\psi_1 = \frac{1}{\sqrt{3}}(u\bar{u} + d\bar{d} + s\bar{s}) \ . \tag{15.7}$$

The mixing relations are often rewritten to exhibit the $u\bar{u} + d\bar{d}$ and $s\bar{s}$ components which decouple for the "ideal" mixing angle θ_i, such that $\tan\theta_i = 1/\sqrt{2}$ (or $\theta_i = 35.3°$). Defining $\alpha = \theta + 54.7°$, one obtains the physical isoscalar state in the flavor basis

Table 15.2: Suggested $q\bar{q}$ quark-model assignments for the lightest mesons made of u, d and s quarks. Mesons in boldface are included in the Meson Summary Table. The wave functions f and f' are given in the text (Eq. (15.8)) and the singlet-octet mixing angles in Table 15.5 below for the well established nonets. The classification of the 0^{++} mesons is tentative: (i) the scalars $a_0(980)$, $K_0^*(700)$, $f_0(980)$ and $f_0(500)$, omitted from the table, are often considered to be four-quark states, see Eq. (15.21) below, but are also proposed for the ground state scalar nonet (see the chapter "Scalar Mesons below 1 GeV" in this *Review*); (ii) the isoscalar 0^{++} mesons $f_0(1370)$, $f_0(1500)$ (not shown) and $f_0(1710)$ are expected to mix. The isoscalar assignments in the 2^1S_0 (0^{-+}) nonet are also tentative. Details and alternative schemes can be found in "Spectroscopy of Light Meson Resonances" in this *Review*.
[a] The $1^{+\pm}$ and $2^{-\pm}$ isospin $\frac{1}{2}$ states mix. In particular, the K_{1A} and K_{1B} are nearly equal mixtures of the $K_1(1270)$ and $K_1(1400)$ [5].
[b] The physical vector mesons are mixtures of 1^3D_1 and 2^3S_1 [6].
[c] The $\eta(1475)$ and $\eta(1405)$ (not shown) may be manifestations of a single state [7].
[d] This state has also been proposed as a tetraquark state [8].

$n^{2s+1}\ell_J$	J^{PC}	I = 1 $u\bar{d}$, $\bar{u}d$, $\frac{1}{\sqrt{2}}(d\bar{d}-u\bar{u})$	I = $\frac{1}{2}$ $u\bar{s}$, $d\bar{s}$; $\bar{d}s$, $\bar{u}s$	I = 0 f'	I = 0 f
1^1S_0	0^{-+}	$\boldsymbol{\pi}$	$\boldsymbol{K}$	$\boldsymbol{\eta}$	$\boldsymbol{\eta'}(958)$
1^3S_1	1^{--}	$\boldsymbol{\rho(770)}$	$\boldsymbol{K^*(892)}$	$\boldsymbol{\phi(1020)}$	$\boldsymbol{\omega(782)}$
1^1P_1	1^{+-}	$\boldsymbol{b_1(1235)}$	$\boldsymbol{K_{1B}}$[a]	$\boldsymbol{h_1(1415)}$	$\boldsymbol{h_1(1170)}$
1^3P_0	0^{++}	$\boldsymbol{a_0(1450)}$	$\boldsymbol{K_0^*(1430)}$	$\boldsymbol{f_0(1710)}$	$\boldsymbol{f_0(1370)}$
1^3P_1	1^{++}	$\boldsymbol{a_1(1260)}$	$\boldsymbol{K_{1A}}$[a]	$\boldsymbol{f_1(1420)}$	$\boldsymbol{f_1(1285)}$
1^3P_2	2^{++}	$\boldsymbol{a_2(1320)}$	$\boldsymbol{K_2^*(1430)}$	$\boldsymbol{f_2'(1525)}$	$\boldsymbol{f_2(1270)}$
1^1D_2	2^{-+}	$\boldsymbol{\pi_2(1670)}$	$\boldsymbol{K_2(1770)}$[a]	$\boldsymbol{\eta_2(1870)}$	$\boldsymbol{\eta_2(1645)}$
1^3D_1	1^{--}	$\boldsymbol{\rho(1700)}$	$\boldsymbol{K^*(1680)}$[b]	$\phi(2170)$[d]	$\boldsymbol{\omega(1650)}$
1^3D_2	2^{--}		$\boldsymbol{K_2(1820)}$[a]		
1^3D_3	3^{--}	$\boldsymbol{\rho_3(1690)}$	$\boldsymbol{K_3^*(1780)}$	$\boldsymbol{\phi_3(1850)}$	$\boldsymbol{\omega_3(1670)}$
1^3F_4	4^{++}	$\boldsymbol{a_4(1970)}$	$\boldsymbol{K_4^*(2045)}$	$f_4(2300)$	$\boldsymbol{f_4(2050)}$
1^3G_5	5^{--}	$\rho_5(2350)$	$K_5^*(2380)$		
2^1S_0	0^{-+}	$\boldsymbol{\pi(1300)}$	$\boldsymbol{K(1460)}$	$\boldsymbol{\eta(1475)}$[c]	$\boldsymbol{\eta(1295)}$
2^3S_1	1^{--}	$\boldsymbol{\rho(1450)}$	$\boldsymbol{K^*(1410)}$[b]	$\boldsymbol{\phi(1680)}$	$\boldsymbol{\omega(1420)}$
2^3P_1	1^{++}	$\boldsymbol{a_1(1640)}$			
2^3P_2	2^{++}	$\boldsymbol{a_2(1700)}$	$\boldsymbol{K_2^*(1980)}$	$\boldsymbol{f_2(1950)}$	$f_2(1640)$

$$f' = \frac{1}{\sqrt{2}}(u\bar{u} + d\bar{d})\cos\alpha - s\bar{s}\ \sin\alpha\ , \tag{15.8}$$

and its orthogonal partner f (replace α by α –90°). Thus for ideal mixing ($\alpha_i = 90°$), the f' becomes pure $s\bar{s}$ and the f pure $u\bar{u} + d\bar{d}$. The mixing angle θ can be derived by diagonalizing the

Table 15.3: $c\bar{c}$ quark-model assignments for the charmonium mesons with established J^{PC} and their corresponding open charm mesons. Mesons in bold face are included in the Meson Summary Table. The open flavor states in the 1^{+-} and 1^{++} rows are mixtures of the $1^{+\pm}$ states.
[a] This meson splits into two states. The ground state scalar meson lies around 2100 MeV [9].
[b] The masses are considerably smaller than most theoretical predictions. They have also been considered as tetraquark or $D^{(*)}K$ molecular states.
[c] Mixtures of the $1\,^3D_1$ and $2\,^3S_1$ states.

$n^{2s+1}\ell_J$	J^{PC}	I = 0	I = 1/2	I = 0
		$c\bar{c}$	$c\bar{u}$, $c\bar{d}$; $\bar{c}u$, $\bar{c}d$	$c\bar{s}$; $\bar{c}s$
$1\,^1S_0$	0^{-+}	$\boldsymbol{\eta_c(1S)}$	$\boldsymbol{D}$	$\boldsymbol{D_s^{\pm}}$
$1\,^3S_1$	1^{--}	$\boldsymbol{J/\psi(1S)}$	$\boldsymbol{D^*}$	$\boldsymbol{D_s^{*\pm}}$
$1\,^3P_0$	0^{++}	$\boldsymbol{\chi_{c0}(1P)}$	$\boldsymbol{D_0^*(2300)}$[a]	$\boldsymbol{D_{s0}^*(2317)^{\pm}}$[b]
$1\,^3P_1$	1^{++}	$\boldsymbol{\chi_{c1}(1P)}$	$D_1(2430)$	$\boldsymbol{D_{s1}(2460)^{\pm}}$[b]
$1\,^1P_1$	1^{+-}	$\boldsymbol{h_c(1P)}$	$\boldsymbol{D_1(2420)}$	$\boldsymbol{D_{s1}(2536)^{\pm}}$
$1\,^3P_2$	2^{++}	$\boldsymbol{\chi_{c2}(1P)}$	$\boldsymbol{D_2^*(2460)}$	$\boldsymbol{D_{s2}^*(2573)^{\pm}}$
$2\,^1S_0$	0^{-+}	$\boldsymbol{\eta_c(2S)}$	$D_0(2500)^0$	$D_{s0}(2590)^+$
$2\,^3S_1$	1^{--}	$\boldsymbol{\psi(2S)}$	$D_1^*(2760)^0$	$\boldsymbol{D_{s1}^*(2700)^{\pm}}$[c]
$1\,^3D_1$	1^{--}	$\boldsymbol{\psi(3770)}$		$D_{s1}^*(2860)^{\pm}$[c]
$1\,^3D_2$	2^{--}	$\boldsymbol{\psi_2(3823)}$	$D_2(2740)^0$	
$2\,^3P_J$	$0^{++}, 1^{++}$	$\chi_{c0}(3860)$		
	2^{++}	$\boldsymbol{\chi_{c2}(3930)}$		
$3\,^3S_1$	1^{--}	$\boldsymbol{\psi(4040)}$		
$2\,^3D_1$	1^{--}	$\boldsymbol{\psi(4160)}$		
$4\,^3S_1$	1^{--}	$\boldsymbol{\psi(4415)}$		
$1\,^3D_3$	3^{--}	$\boldsymbol{\psi_3(3842)}$	$D_3^*(2750)$	$D_{s3}^*(2860)^{\pm}$

mass matrix

$$\begin{pmatrix} m_8 & m_{81} \\ m_{18} & m_1 \end{pmatrix}.$$

The mass eigenvalues are $m_{f'}$ and m_f. The mixing angle is given by

$$\tan\theta = \frac{m_8 - m_{f'}}{m_{81}} \ .$$

Calculating m_8 and m_{81} from the wave functions Eq. (15.6) and Eq. (15.7), and expressing the quark masses as a function of the I = 1/2 and I = 1 meson masses, one obtains

$$\tan\theta = \frac{4m_K - m_a - 3m_{f'}}{2\sqrt{2}(m_a - m_K)} \ , \tag{15.9}$$

which also determines the sign of θ. Alternatively, one can express the mixing angle as a function of all nonet masses. The octet mass is given by

$$m_8 = m_{f'}\cos^2\theta + m_f \sin^2\theta$$

Table 15.4: $b\bar{b}$ quark-model assignments for the bottomonium mesons with established J^{PC} and their corresponding open bottom mesons.

$n^{2s+1}\ell_J$	J^{PC}	I = 0 $b\bar{b}$	I = $\frac{1}{2}$ $b\bar{u}$, $b\bar{d}$; $\bar{b}u$, $\bar{b}d$	I = 0 $b\bar{s}$; $\bar{b}s$	I = 0 $b\bar{c}$; $\bar{b}c$
$1\,^1S_0$	0^{-+}	$\boldsymbol{\eta_b(1S)}$	$\boldsymbol{B}$	$\boldsymbol{B_s^0}$	$\boldsymbol{B_c^\pm}$
$1\,^3S_1$	1^{--}	$\boldsymbol{\Upsilon(1S)}$	$\boldsymbol{B^*}$	$\boldsymbol{B_s^*}$	
$1\,^3P_0$	0^{++}	$\boldsymbol{\chi_{b0}(1P)}$			
$1\,^3P_1$	1^{++}	$\boldsymbol{\chi_{b1}(1P)}$			
$1\,^1P_1$	1^{+-}	$\boldsymbol{h_b(1P)}$	$\boldsymbol{B_1(5721)}$	$\boldsymbol{B_{s1}(5830)^0}$	
$1\,^3P_2$	2^{++}	$\boldsymbol{\chi_{b2}(1P)}$	$\boldsymbol{B_2^*(5747)}$	$\boldsymbol{B_{s2}^*(5840)^0}$	
$2\,^1S_0$	0^{-+}	$\eta_b(2S)$			$\boldsymbol{B_c(2S)^\pm}$
$2\,^3S_1$	1^{--}	$\boldsymbol{\Upsilon(2S)}$			
$1\,^3D_2$	2^{--}	$\boldsymbol{\Upsilon_2(1D)}$			
$2\,^3P_J$	$0,1,2^{++}$	$\boldsymbol{\chi_{b0,1,2}(2P)}$			
$2\,^1P_1$	1^{+-}	$\boldsymbol{h_b(2P)}$			
$3\,^3S_1$	1^{--}	$\boldsymbol{\Upsilon(3S)}$			
$3\,^3P_J$	$0,1,2^{++}$	$\boldsymbol{\chi_{b1,2}(3P)}$			
$4\,^3S_1$	1^{--}	$\boldsymbol{\Upsilon(4S)}$			

whence

$$\tan^2\theta = \frac{4m_K - m_a - 3m_{f'}}{-4m_K + m_a + 3m_f} \ . \tag{15.10}$$

Eliminating θ from Eq. (15.9) and Eq. (15.10) leads to the sum rule [10]

$$(m_f + m_{f'})(4m_K - m_a) - 3m_f m_{f'} = 8m_K^2 - 8m_K m_a + 3m_a^2. \tag{15.11}$$

This relation is verified for the ground-state vector mesons. We identify the $\phi(1020)$ with the f' and the $\omega(783)$ with the f. Thus

$$\phi(1020) = \psi_8 \cos\theta_V - \psi_1 \sin\theta_V \ , \tag{15.12}$$

$$\omega(782) = \psi_8 \sin\theta_V + \psi_1 \cos\theta_V \ , \tag{15.13}$$

with the vector mixing angle $\theta_V = 36.5°$ from Eq. (15.10), very close to ideal mixing. Thus $\phi(1020)$ is nearly pure $s\bar{s}$. For ideal mixing, Eq. (15.9) and Eq. (15.10) lead to the relations

$$m_K = \frac{m_f + m_{f'}}{2} \ , \quad m_a = m_f \ , \tag{15.14}$$

which are satisfied for the vector mesons.

The situation for the pseudoscalar and scalar mesons is not so clear cut, either theoretically or experimentally. For the pseudoscalars, the mixing angle is small. This can be understood qualitatively via gluon-line counting of the mixing process. The size of the mixing process between the nonstrange and strange mass bases scales as α_s^2, not α_s^3, because of two rather than three gluon exchange as it does for the vector mesons. It may also be that the lightest isoscalar pseudoscalars mix more strongly with excited states or with states of substantial non-$\bar{q}q$ content, as will be discussed below.

In fact a large mixing from hadronic loops is expected for scalar mesons, no matter what model is assumed for $q\bar{q}$ pair production [11]. A variety of analysis methods lead to similar results: First, for these states, Eq. (15.11) is satisfied only approximately. Then Eq. (15.9) and Eq. (15.10) lead to somewhat different values for the mixing angle. Identifying the η with the f' one gets

$$\eta = \psi_8 \cos\theta_P - \psi_1 \sin\theta_P \ , \tag{15.15}$$

$$\eta' = \psi_8 \sin\theta_P + \psi_1 \cos\theta_P \ . \tag{15.16}$$

Following chiral perturbation theory, the meson masses in the mass formulae (Eq. (15.9) and Eq. (15.10)) might be replaced by their squares. Table 15.5 lists the mixing angle $\theta_{\rm lin}$ from Eq. (15.10) (using the neutral members of the nonets) and the corresponding $\theta_{\rm quad}$ obtained by replacing the meson masses by their squares throughout. The mixing angles in the 1^{--}, 2^{++} and 3^{--} nonets are not far from ideal, while larger $s\bar{s}$-$(u\bar{u}+d\bar{d})$ mixing is predicted from hadronic loops in the 0^{++}, 0^{-+} and $1^{+\pm}$ nonets [11].

Table 15.5: Singlet-octet mixing angles for the well established nonets from the linear mass formula Eq. (15.10) and its quadratic version in which the masses are squared. The 1^{++} and 1^{+-} nonet mixing angles depend on the mixing angle θ_{K_1} between K_{1A} and K_{1B}. The recommended values are $\sim$23° and $\sim$28° for 1^{++} and 1^{+-}, respectively, with $\theta_{K_1}\sim$35° [5].

$n^{2s+1}\ell_J$	J^{PC}	$\theta_{\rm quad}$ [°]	$\theta_{\rm lin}$ [°]
1^1S_0	0^{-+}	−11.3	−24.5
1^3S_1	1^{--}	39.2	36.5
1^3P_2	2^{++}	29.6	28.0
1^3D_3	3^{--}	31.8	30.8

The pseudoscalar mixing angle θ_P can also be measured by comparing the partial widths for radiative J/ψ decay into a vector and a pseudoscalar [12], radiative $\phi(1020)$ decay into η and η' [13], radiative decays between pseudoscalar and vector mesons [14], or $\bar{p}p$ annihilation at rest into a pair of vector and pseudoscalar or into two pseudoscalars [15,16]. One obtains a mixing angle between –10° and –20°. More recently, a lattice QCD simulation, Ref. [17], has successfully reproduced the masses of the η and η', and as a byproduct find a mixing angle $\theta_{lin} = -14.1(2.8)°$. We return to this point in Sec. 15.8.

The nonet mixing angles can be measured in $\gamma\gamma$ collisions, *e.g.*, for the 0^{-+}, 0^{++}, and 2^{++} nonets. In the quark model, the amplitude for the coupling of neutral mesons to two photons is proportional to $\sum_i Q_i^2$, where Q_i is the charge of the i-th quark. The 2γ partial width of an isoscalar meson with mass m is then given in terms of the mixing angle α by

$$\Gamma_{2\gamma} = C(5\cos\alpha - \sqrt{2}\sin\alpha)^2 m^3 \ , \tag{15.17}$$

for f' and f ($\alpha \to \alpha - 90°$). The coupling C may depend on the meson mass. It is often assumed to be a constant in the nonet. For the isovector a, one finds $\Gamma_{2\gamma} = 9\ C\ m^3$. Thus the members of an ideally mixed nonet couple to 2γ with partial widths in the ratios $f : f' : a = 25 : 2 : 9$. For tensor mesons, one finds from the ratios of the measured 2γ partial widths for the $f_2(1270)$ and $f_2'(1525)$ mesons a mixing angle α_T of $(81\pm 1)°$, or $\theta_T = (27 \pm 1)°$, in accord with the linear mass formula. For the pseudoscalars, one finds from the ratios of partial widths $\Gamma(\eta' \to 2\gamma)/\Gamma(\eta \to 2\gamma)$ a mixing angle $\theta_P = (-18 \pm 2)°$, while the ratio $\Gamma(\eta' \to 2\gamma)/\Gamma(\pi^0 \to 2\gamma)$ leads to $\sim$ –24 °. SU(3) breaking effects for pseudoscalars are discussed in [18].

The partial width Γ for the decay of a scalar or a tensor meson into a pair of pseudoscalar mesons is model-dependent. Following Ref. [19],

$$\Gamma = C \times \gamma^2 \times |F(q)|^2 \times q \ , \tag{15.18}$$

where C is a nonet constant, q the momentum of the decay products, $F(q)$ a form factor, and γ^2 the SU(3) coupling. Details and explicit expressions for γ^2 and $F(q)$ are given in "Spectroscopy of Light Meson Resonances". The decay of a $q\bar{q}$ meson into a pair of mesons involves the creation of a $q\bar{q}$ pair, and SU(3) symmetry assumes that the matrix elements for the creation of $s\bar{s}$, $u\bar{u}$, and $d\bar{d}$ pairs are equal. An excellent fit to the tensor meson decay widths is obtained assuming SU(3) symmetry and a pseudoscalar mixing angle $\theta_P \simeq -17\ ^\circ$ [19].

The analysis of resonances is complicated by the presence of thresholds such as $K\bar{K}$ in $a_0(980) \to \eta\pi$ or $f_0(980) \to \pi\pi$, which affect the resonance masses and widths. A particularly nasty kinematic effect is the triangle singularity in which one of the primary decay daughters in turn decays and is emitted backwards, catching up and scattering with the second primary product. This mechanism generates fake peaks in the final state and has been proposed as alternative explanation for several meson (and baryon) signals. Prominent examples are the $\eta(1475) \to K^*(\to K\pi)\bar{K}$ and $\eta(1410) \to a_0(980)(\to \eta\pi)\pi$ signals which could be due to one single state [7] (see also Table 15.2).

15.4 Exotic mesons

The existence of a light nonet composed of four quarks (tetraquarks) with masses below 1 GeV was suggested a long time ago [20,21]. Coupling two triplets of light quarks u, d, and s, one obtains nine states, of which the six symmetric ($uu,\ dd,\ ss,\ ud+du,\ us+su,\ ds+sd$) form the six dimensional representation **6**, while the three antisymmetric ($ud-du,\ us-su,\ ds-sd$) form the three dimensional representation $\overline{\mathbf{3}}$ of SU(3):

$$\mathbf{3} \otimes \mathbf{3} = \mathbf{6} \oplus \overline{\mathbf{3}} \ . \tag{15.19}$$

Hence for tetraquarks one gets the reduction

$$\begin{aligned} &\mathbf{3} \otimes \mathbf{3} \otimes \overline{\mathbf{3}} \otimes \overline{\mathbf{3}} \\ &= \mathbf{6} \oplus \overline{\mathbf{3}} \otimes \overline{\mathbf{6}} \otimes \mathbf{3} \\ &= \overline{\mathbf{3}} \otimes \mathbf{3} \oplus \mathbf{6} \otimes \overline{\mathbf{6}} \oplus \mathbf{6} \otimes \mathbf{3} \oplus \overline{\mathbf{3}} \otimes \overline{\mathbf{6}} \\ &= \mathbf{9} \oplus \mathbf{36} \oplus \mathbf{18} \oplus \overline{\mathbf{18}}. \end{aligned} \tag{15.20}$$

Combining with spin and color and requiring antisymmetry for diquarks and antidiquarks, one finds for ground states (zero angular momenta) that the most deeply bound tetraquarks (and hence the lightest ones) lie in the nonet and are scalar mesons (see also [4]). The average mass is estimated to be around 900 MeV from the mass differences between the ρ and π masses. Letting the strange quark determine the mass splittings one obtains a mass inverted spectrum with a light isosinglet, a medium heavy isodoublet and a heavy isotriplet + isosinglet. It is then tempting to identify these mesons as the lightest scalars

$$\begin{aligned} f_0(500) &= \bar{u}\bar{d}ud, \\ K_0^*(700) &= (\bar{s}\bar{d}ud, \bar{s}\bar{u}ud) \ \text{ and } \ (\bar{u}\bar{d}us, \bar{u}\bar{d}ds), \\ a_0(980) &= (us\bar{d}\bar{s}, \frac{1}{\sqrt{2}}[u\bar{u} - d\bar{d}]s\bar{s}, \bar{u}\bar{s}ds), \\ f_0(980) &= \frac{1}{\sqrt{2}}[u\bar{u} + d\bar{d}]s\bar{s}. \end{aligned} \tag{15.21}$$

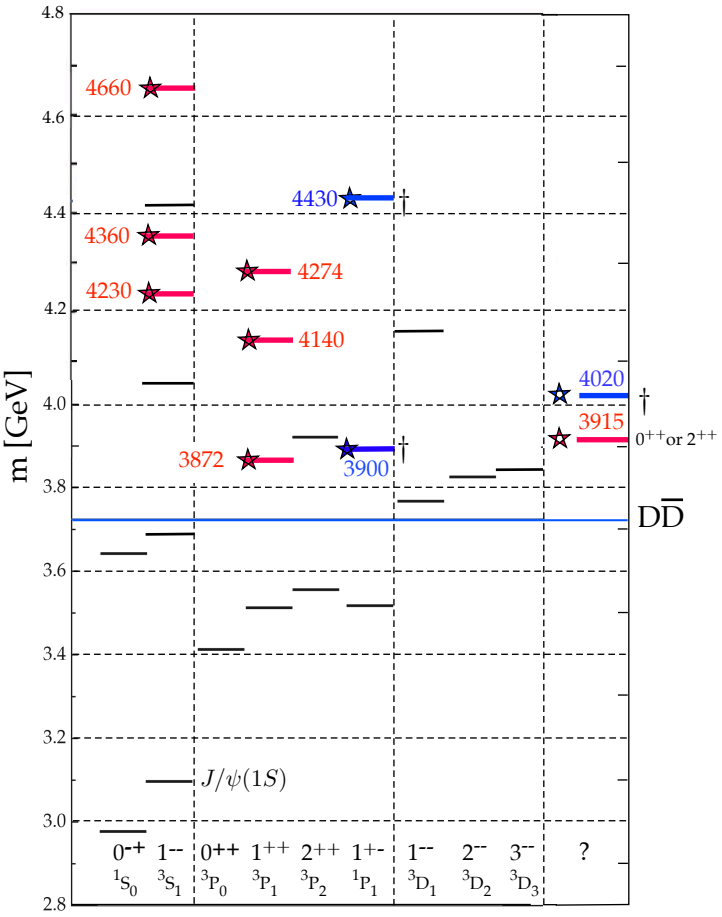

Figure 15.2: Established states populating the charmonium spectrum that are listed in the Summary Tables. The $c\bar{c}$ states are shown in black, the exotic ones are tagged by stars (red for the isoscalars, blue for the isovectors). The quantum numbers of the two states in the right column are not firmly established.

In alternative schemes these states build the lightest $q\bar{q}$ scalar nonet (for details see "Scalar mesons below 1 GeV" in this *"Review"*).

A plethora of new states have been reported in the charmonium and bottomonium spectra. The most prominent one is the $\chi_{c1}(3872)$ (formerly $X(3872)$), first observed in 2003 in B-decays in the final state $J/\psi\,\pi^+\pi^-$ (see Fig. 15.2). Even more remarkable is the observation of isovector (charged) candidates decaying into $c\bar{c}$ plus a charged pion, such as the $Z^{\pm}(4430)$ decaying into $\psi(2S)\pi^{\pm}$, which a priori excludes an interpretation as true $c\bar{c}$ (charmonium) state. Similar states are also observed in the bottomonium spectrum. Some of these states may be tetraquarks (e.g. $cq\bar{c}\bar{q}$), molecular structures (e.g. $c\bar{q}\bar{c}q$) made of pairs of mesons such as D, D_s and D^*, D_s^* excitations, or their B and B^* counterparts. They could also be mimicked by kinematical effects such as triangle singularities. Details and references can be found in recent reviews [23], [24] and in the review "Heavy non-$q\bar{q}$ Mesons" .

QCD predicts the existence of extra isoscalar mesons which cannot be addressed by the quark model. In the pure gauge theory they contain only gluons, and are called glueballs. The ground state glueball is predicted by lattice gauge theories to be 0^{++}, the first excited state 2^{++}. Errors on the mass predictions are large. From Ref. [25] one obtains 1750 (50) (80) MeV for the mass of

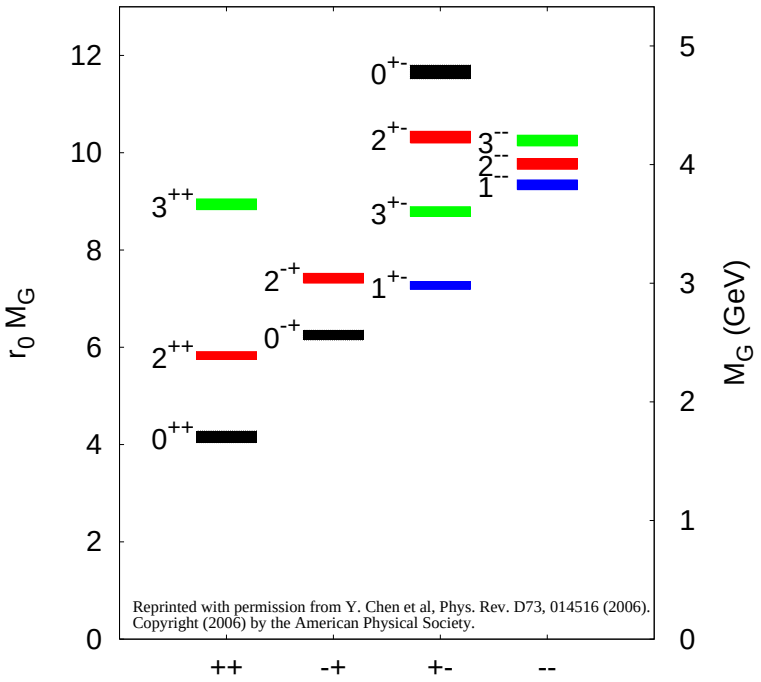

Figure 15.3: Predicted glueball mass spectrum from the lattice in quenched approximation (from [22]).

the lightest 0^{++} glueball from quenched QCD. As an example for the glueball mass spectrum, we show in Fig. 15.3 a calculation from Ref. [22]. A mass of 1710 MeV is predicted for the ground state, also with an error of about 100 MeV. Earlier work by other groups produced masses at 1650 MeV [26] and 1550 MeV [27] (see also [28]. The first excited state has a mass of about 2.4 GeV, and the lightest glueball with exotic quantum numbers (2^{+-}) has a mass of about 4 GeV.

These calculations are made in the so-called "quenched approximation" which neglects $q\bar{q}$ loops. However, both glue and $q\bar{q}$ states couple to singlet scalar mesons. Therefore glueballs will mix with nearby $q\bar{q}$ states of the same quantum numbers. For example, the two isoscalar 0^{++} mesons around 1500 MeV will mix with the pure ground state glueball to generate the observed physical states $f_0(1370)$, $f_0(1500)$, and $f_0(1710)$ [19, 29]. The first results from lattice calculations, which include these effects, indicate that the mass shifts are small. We return to a discussion of this point in Sec. 15.8, see also Fig. 15.15.

The existence of three singlet scalar mesons around 1.5 GeV suggests additional degrees of freedom such as glue, since only two mesons are predicted in this mass range. The $f_0(1500)$ [19,29] or, alternatively, the $f_0(1710)$ [26], have been proposed as candidates for the scalar glueball, both states having considerable mixing also with the $f_0(1370)$. Other mixing schemes, in particular with the $f_0(500)$ and the $f_0(980)$, have also been proposed [30]. According to a holographic model of low-energy QCD scalar glueballs decay strongly into kaons and η mesons, in good agreement with data on the $f_0(1710)$ [31]. Details can be found in the review "Spectroscopy of Light Meson Resonances" and in Ref. [32]. See also the review "Scalar Mesons below 1 GeV" in this *Review*.

Mesons made of $q\bar{q}$ pairs bound by excited gluons g, the hybrid states $q\bar{q}g$, are also predicted. They should lie in the 1.9 GeV mass region, according to gluon flux tube models [33]. Lattice QCD also predicts the lightest hybrid, an exotic 1^{-+}, at a mass of 1.8 to 1.9 GeV [34]. However, the bag model predicts four nonets, among them an exotic 1^{-+} around or above 1.4 GeV [35, 36]. There are so far two candidates for exotic states with quantum numbers 1^{-+}, the $\pi_1(1400)$ and

$\pi_1(1600)$, which could be hybrids or four-quark states. However, a recent combined re-analysis of π_1 production in diffractive $\pi^- p$ interaction and low energy $\bar{p}p$ annihilation leads to a single pole at ∼1560 MeV with a width of ∼390 MeV, although a two-pole scenario cannot be excluded [37]. (See the review "Spectroscopy of Light Meson Resonances" in this *Review* and Ref. [32].)

15.5 Baryons: qqq states

Baryons are fermions with baryon number $\mathcal{B} = 1$, *i.e.*, in the most general case, they are composed of three quarks plus any number of quark - antiquark pairs. Until recently, all established baryons were 3-quark (qqq) configurations, which we mainly discuss in this section. However, in 2015 the LHCb collaboration published first evidence for charmed 'pentaquark' states of minimal quark content $c\bar{c}uud$ at invariant masses close to 4.4 GeV [38]. More refined LHCb experiments have revealed evidence for three such states called $P_c(4312)^+$, $P_c(4440)^+$, and $P_c(4457)^+$ [39]. These states are located close to the thresholds of the production of ordinary baryon-meson pairs like $\Sigma_c^+ \bar{D}^0$ and $\Sigma_c^+ \bar{D}^{\star 0}$ and are consistent with the predictions [40, 41] in terms of molecular-like states. A nice overview on the discussion of pentaquark and tetraquark states is given in Ref. [42].

The color part of baryon state functions is an SU(3) singlet, a completely antisymmetric state of the three colors. Since the quarks are fermions, the state function must be antisymmetric under interchange of any two equal-mass quarks (up and down quarks in the limit of isospin symmetry). Thus it can be written as

$$|\, qqq \,\rangle_A = |\, \text{color} \,\rangle_A \times |\, \text{space, spin, flavor} \,\rangle_S, \tag{15.22}$$

where the subscripts S and A indicate symmetry or antisymmetry under interchange of any two equal-mass quarks. Note the contrast with the state function for the three nucleons in ^{3}H or ^{3}He:

$$|\, NNN \,\rangle_A = |\, \text{space, spin, isospin} \,\rangle_A. \tag{15.23}$$

This difference has major implications for internal structure, magnetic moments, *etc.* (For a nice discussion, see Ref. [43].)

15.5.1 *Light baryons*

The "ordinary" baryons are made up of u, d, and s quarks. The three flavors imply an approximate flavor SU(3), which requires that baryons made of these quarks belong to the multiplets on the right side of

$$\mathbf{3} \otimes \mathbf{3} \otimes \mathbf{3} = \mathbf{10}_S \oplus \mathbf{8}_M \oplus \mathbf{8}_M \oplus \mathbf{1}_A \tag{15.24}$$

(see the section on "SU(n) Multiplets and Young Diagrams" in this *Review*). Here the subscripts indicate symmetric, mixed-symmetry, or antisymmetric states under interchange of any two quarks. The **1** is a uds state (Λ_1), and the octet contains a similar state (Λ_8). If these have the same spin and parity, they can mix. The mechanism is the same as for the mesons (see above). In the ground state multiplet, the SU(3) flavor singlet Λ_1 is forbidden by Fermi statistics. The section on "SU(3) Isoscalar Factors and Representation Matrices," shows how relative decay rates in, say, $\mathbf{10} \to \mathbf{8} \otimes \mathbf{8}$ decays may be calculated.

For the "ordinary" baryons (no c or b quark), flavor and spin may be combined in an approximate flavor-spin SU(6), in which the six basic states are $d\uparrow$, $d\downarrow$, $\cdots$, $s\downarrow$ ($\uparrow, \downarrow$ = spin up, down). Then the baryons belong to the multiplets on the right side of

$$\mathbf{6} \otimes \mathbf{6} \otimes \mathbf{6} = \mathbf{56}_S \oplus \mathbf{70}_M \oplus \mathbf{70}_M \oplus \mathbf{20}_A. \tag{15.25}$$

These SU(6) multiplets decompose into flavor SU(3) multiplets as follows:

$$\mathbf{56} = {}^4\mathbf{10} \oplus {}^2\mathbf{8} \tag{15.26a}$$

$$\mathbf{70} = {}^2\mathbf{10} \oplus {}^4\mathbf{8} \oplus {}^2\mathbf{8} \oplus {}^2\mathbf{1} \tag{15.26b}$$

$$\mathbf{20} = {}^2\mathbf{8} \oplus {}^4\mathbf{1}, \tag{15.26c}$$

where the superscript $(2S + 1)$ gives the net spin S of the quarks for each particle in the SU(3) multiplet. The $J^P = 1/2^+$ octet containing the nucleon and the $J^P = 3/2^+$ decuplet containing the $\Delta(1232)$ together make up the "ground-state" 56-plet, in which the orbital angular momenta between the quark pairs are zero (so that the spatial part of the state function is trivially symmetric). The **70** and **20** require some excitation of the spatial part of the state function in order to make the overall state function symmetric. States with nonzero orbital angular momenta are classified in SU(6)⊗O(3) supermultiplets.

It is useful to classify the baryons into bands that have the same number N of quanta of excitation. Each band consists of a number of supermultiplets, specified by (D, L_N^P), where D is the dimensionality of the SU(6) representation, L is the total quark orbital angular momentum, and P is the total parity. Supermultiplets contained in bands up to N = 12 are given in Ref. [44]. The N = 0 band, which contains the nucleon and $\Delta(1232)$, consists only of the $(56,0_0^+)$ supermultiplet. The N = 1 band consists only of the $(70,1_1^-)$ multiplet and contains the negative-parity baryons with masses below about 1.9 GeV. The N = 2 band contains five supermultiplets: $(56,0_2^+)$, $(70,0_2^+)$, $(56,2_2^+)$, $(70,2_2^+)$, and $(20,1_2^+)$.

The wave functions of the non-strange baryons in the harmonic oscillator basis are often labeled by $|X^{2S+1}L_\pi J^P\rangle$, where S, L, J, P are as above, $X = N$ or Δ, and $\pi = S, M$ or A denotes the symmetry of the spatial wave function. The possible model states for the bands with N=0,1,2 are given in Table 15.7. The assignment of experimentally observed states is only complete and well established up to the N=1 band. Some more tentative assignments for higher multiplets are suggested in [45].

In Table 15.6, quark-model assignments are given for many of the established baryons whose SU(6)⊗O(3) compositions are relatively unmixed. One must, however, keep in mind that apart from the mixing of the Λ singlet and octet states, states with same J^P but different L, S combinations can also mix. In the quark model with one-gluon exchange motivated interactions, the size of the mixing is determined by the relative strength of the tensor term with respect to the contact term (see below). The mixing is more important for the decay patterns of the states than for their positions. An example are the lowest lying $(70, 1_1^-)$ states with J^P=1/2$^-$ and 3/2$^-$. The physical states are:

$$|\,N(1535)1/2^-\rangle = \cos(\Theta_S)|N^2P_M1/2^-\rangle - \sin(\Theta_S)|N^4P_M1/2^-\rangle \tag{15.27}$$

$$|\,N(1520)3/2^-\rangle = \cos(\Theta_D)|N^2P_M3/2^-\rangle - \sin(\Theta)_D|N^4P_M3/2^-\rangle \tag{15.28}$$

and the orthogonal combinations for $N(1650)1/2^-$ and $N(1700)3/2^-$. The mixing is large for the J^P=1/2$^-$ states ($\Theta_S \approx$ -32^o), but small for the J^P=3/2$^-$ states ($\Theta_D \approx +6^o$) [47–49].

All baryons of the ground state multiplets are known. Many of their properties, in particular their masses, are in good agreement even with the most basic versions of the quark model, including harmonic (or linear) confinement and a spin-spin interaction, which is responsible for the octet - decuplet mass shifts. A consistent description of the ground-state electroweak properties, however, requires refined relativistic constituent quark models.

The situation for the excited states is much less clear. The assignment of some experimentally observed states with strange quarks to model configurations is only tentative and in many cases candidates are completely missing. Melde, Plessas and Sengl [46] have calculated baryon properties in relativistic constituent quark models, using one-gluon exchange and Goldstone-boson exchange for the modeling of the hyperfine interactions (see Sec. 15.7 on Dynamics). Both types of models give qualitatively comparable results, and underestimate in general experimentally observed decay

Table 15.6: Quark-model assignments for some of the known baryons in terms of a flavor-spin SU(6) basis. Only the dominant representation is listed. Assignments for several states, especially for the $\Lambda(1810)$, $\Lambda(2350)$, $\Xi(1820)$, and $\Xi(2030)$, are merely educated guesses.
† suggestions for assignments and re-assignments from Ref. [46].

J^P	(D, L_N^P)	S	Octet members				Singlets
$1/2^+$	$(56,0_0^+)$	1/2	$N(939)$	$\Lambda(1116)$	$\Sigma(1193)$	$\Xi(1318)$	
$1/2^+$	$(56,0_2^+)$	1/2	$N(1440)$	$\Lambda(1600)$	$\Sigma(1660)$	$\Xi(1690)^\dagger$	
$1/2^-$	$(70,1_1^-)$	1/2	$N(1535)$	$\Lambda(1670)$	$\Sigma(1620)$	$\Xi(?)$	$\Lambda(1405)$
					$\Sigma(1560)^\dagger$		
$3/2^-$	$(70,1_1^-)$	1/2	$N(1520)$	$\Lambda(1690)$	$\Sigma(1670)$	$\Xi(1820)$	$\Lambda(1520)$
$1/2^-$	$(70,1_1^-)$	3/2	$N(1650)$	$\Lambda(1800)$	$\Sigma(1750)$	$\Xi(?)$	
					$\Sigma(1620)^\dagger$		
$3/2^-$	$(70,1_1^-)$	3/2	$N(1700)$	$\Lambda(?)$	$\Sigma(1940)^\dagger$	$\Xi(?)$	
$5/2^-$	$(70,1_1^-)$	3/2	$N(1675)$	$\Lambda(1830)$	$\Sigma(1775)$	$\Xi(1950)^\dagger$	
$1/2^+$	$(70,0_2^+)$	1/2	$N(1710)$	$\Lambda(1810)$	$\Sigma(1880)$	$\Xi(?)$	$\Lambda(1810)^\dagger$
$3/2^+$	$(56,2_2^+)$	1/2	$N(1720)$	$\Lambda(1890)$	$\Sigma(?)$	$\Xi(?)$	
$5/2^+$	$(56,2_2^+)$	1/2	$N(1680)$	$\Lambda(1820)$	$\Sigma(1915)$	$\Xi(2030)$	
$7/2^-$	$(70,3_3^-)$	1/2	$N(2190)$	$\Lambda(?)$	$\Sigma(?)$	$\Xi(?)$	$\Lambda(2100)$
$9/2^-$	$(70,3_3^-)$	3/2	$N(2250)$	$\Lambda(?)$	$\Sigma(?)$	$\Xi(?)$	
$9/2^+$	$(56,4_4^+)$	1/2	$N(2220)$	$\Lambda(2350)$	$\Sigma(?)$	$\Xi(?)$	
			Decuplet members				
$3/2^+$	$(56,0_0^+)$	3/2	$\Delta(1232)$	$\Sigma(1385)$	$\Xi(1530)$	$\Omega(1672)$	
$3/2^+$	$(56,0_2^+)$	3/2	$\Delta(1600)$	$\Sigma(1690)^\dagger$	$\Xi(?)$	$\Omega(?)$	
$1/2^-$	$(70,1_1^-)$	1/2	$\Delta(1620)$	$\Sigma(1750)^\dagger$	$\Xi(?)$	$\Omega(?)$	
$3/2^-$	$(70,1_1^-)$	1/2	$\Delta(1700)$	$\Sigma(?)$	$\Xi(?)$	$\Omega(?)$	
$5/2^+$	$(56,2_2^+)$	3/2	$\Delta(1905)$	$\Sigma(?)$	$\Xi(?)$	$\Omega(?)$	
$7/2^+$	$(56,2_2^+)$	3/2	$\Delta(1950)$	$\Sigma(2030)$	$\Xi(?)$	$\Omega(?)$	
$11/2^+$	$(56,4_4^+)$	3/2	$\Delta(2420)$	$\Sigma(?)$	$\Xi(?)$	$\Omega(?)$	

widths. Nevertheless, in particular on the basis of the observed decay patterns, the authors have assigned some additional states with strangeness to the SU(3) multiplets and suggest re-assignments for a few others. Among the new assignments are states with weak experimental evidence (two or three star ratings) and partly without firm spin/parity assignments, so that further experimental efforts are necessary before final conclusions can be drawn. We have added their suggestions in Table 15.6.

In the non-strange sector there are two main problems which are illustrated in Fig. 15.4, where the experimentally observed excitation spectrum of the nucleon (N and Δ resonances) is compared to the results of a typical quark model calculation [50]. The lowest states from the N=2 band, the $N(1440)1/2^+$, and the $\Delta(1600)3/2^+$, appear lower than the negative parity states from the N=1 band (see Table 15.7) and much lower than predicted by most models. Also negative parity Δ states from the N=3 band ($\Delta(1900)1/2^-$, $\Delta(1940)3/2^-$, and $\Delta(1930)5/2-$) are too low in energy. The low lying states show a clustering in groups of levels around 1700 MeV and 1900 MeV for $N^\star$ states and around 1900 MeV for Δ states which is not reflected in models.

Table 15.7: N and Δ states in the N=0,1,2 harmonic oscillator bands. L^P denotes angular momentum and parity, S the three-quark spin and 'sym'=A,S,M the symmetry of the spatial wave function. Listed are all possible spin/parity combinations and assignments of experimentally observed states. Only dominant components are indicated. Assignments in the N=2 band are partly tentative.

N	sym	L^P	S	$N(I=1/2)$			
2	A	1^+	1/2	$1/2^+$	$3/2^+$	-	-
2	M	2^+	3/2	$1/2^+$	$3/2^+$	$5/2^+$	$7/2^+$
2	M	2^+	1/2	-	$3/2^+$	$5/2^+$	-
2	M	0^+	3/2	-	$3/2^+$	-	-
2	M	0^+	1/2	$1/2^+$ $N(1710)$	-	-	-
2	S	2^+	3/2	-	-	-	-
2	S	2^+	1/2	-	$3/2^+$ $N(1720)$	$5/2^+$ $N(1680)$	-
2	S	0^+	3/2	-	-	-	-
2	S	0^+	1/2	$1/2^+$ $N(1440)$	-	-	-
1	M	1^-	3/2	$1/2^-$ $N(1650)$	$3/2^-$ $N(1700)$	$5/2^-$ $N(1675)$	-
1	M	1^-	1/2	$1/2^-$ $N(1535)$	$3/2^-$ $N(1520)$	-	-
0	S	0^+	3/2	-	-	-	-
0	S	0^+	1/2	$1/2^+$ $N(938)$	-	-	-
N	sym	L^P	S	$\Delta(I=3/2)$			
2	A	1^+	1/2	-	-	-	-
2	M	2^+	3/2	-	-	-	-
2	M	2^+	1/2	-	$3/2^+$	$5/2^+$	-
2	M	0^+	3/2	-	-	-	-
2	M	0^+	1/2	$1/2^+$ $\Delta(1750)$	-	-	-
2	S	2^+	3/2	$1/2^+$ $\Delta(1910)$	$3/2^+$ $\Delta(1920)$	$5/2^+$ $\Delta(1905)$	$7/2^+$ $\Delta(1950)$
2	S	2^+	1/2	-	-	-	-
2	S	0^+	3/2	-	$3/2^+$ $\Delta(1600)$	-	-
2	S	0^+	1/2	-	-	-	-
1	M	1^-	3/2	-	-	-	-
1	M	1^-	1/2	$1/2^-$ $\Delta(1620)$	$3/2^-$ $\Delta(1700)$	-	-
0	S	0^+	3/2	-	$3/2^+$ $\Delta(1232)$	-	
0	S	0^+	1/2	-	-	-	-

Furthermore, many more states are predicted than observed. This has been known for a long time as the 'missing resonance' problem [47]. Up to an excitation energy of 2.4 GeV, about 45 N states are predicted, but only 20 are established (four- or three-star; see Note on N and Δ Resonances for the rating of the status of resonances) and 5 are tentative (two- or one-star). Even for the N=2 band, up to now only half of the predicted states have been observed. However, there is some recent progress. The total number of states has not much changed but the number of states with four- or three-star rating has increased from 14 to 20 compared to the 2018 PDG particle listings. Most of this progress is due to the programs concentrating on the study of meson photoproduction reactions, while the most recent partial wave analysis of elastic pion scattering and charge exchange data by Arndt and collaborators [52] found no evidence for almost half of

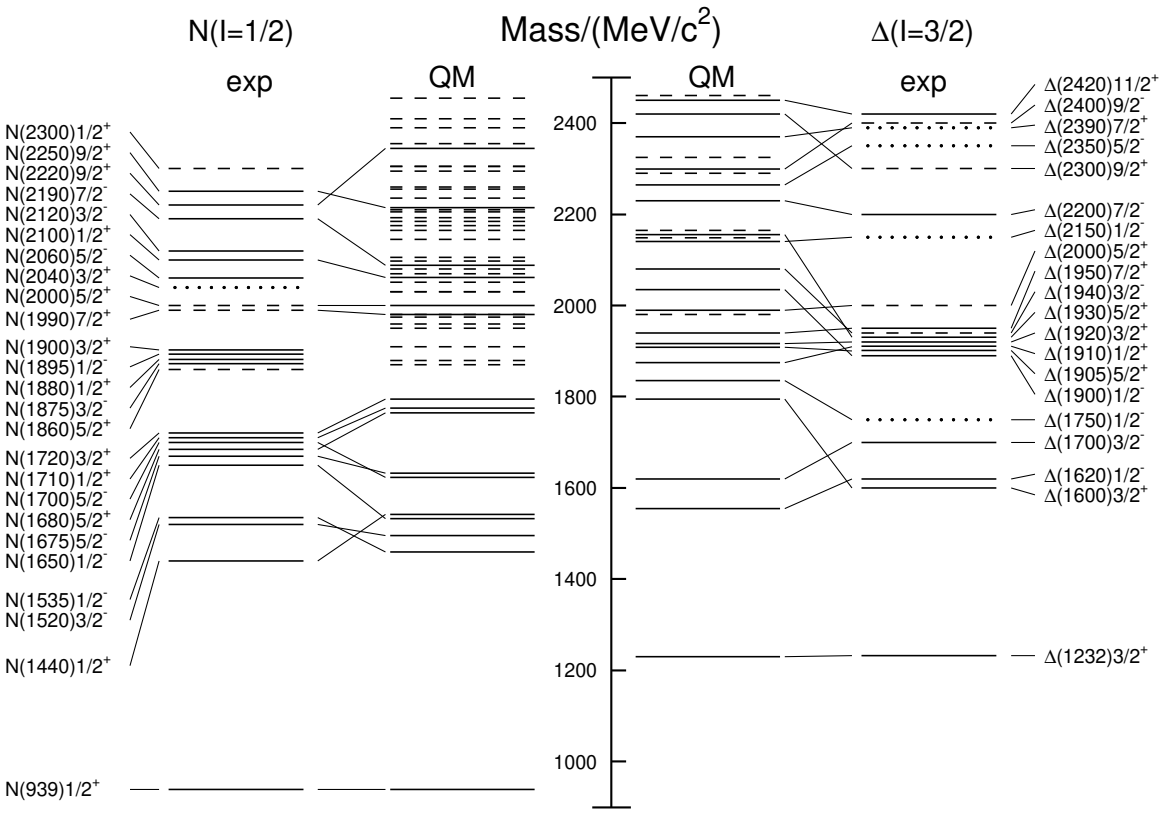

Figure 15.4: Excitation spectrum of the nucleon. Compared are the positions of the excited states identified in experiment, to those predicted by a relativized quark model calculation. Left hand side: isospin $I = 1/2$ N-states, right hand side: isospin $I = 3/2$ Δ-states. Experimental: (columns labeled 'exp'), three- and four-star states are indicated by full lines (two-star dashed lines, one-star dotted lines). At the very left and right of the figure, the spectroscopic notation of these states is given. Quark model [50, 51]: (columns labeled 'QM'), all states for the N=1,2 bands, low-lying states for the N=3,4,5 bands. Full lines: at least tentative assignment to observed states, dashed lines: so far no observed counterparts. Many of the assignments between predicted and observed states are highly tentative.

the states listed in this review (and included in Fig. 15.4). Such analyses are of course biased against resonances which couple only weakly to the $N\pi$ channel. Quark model predictions for the couplings to other hadronic channels and to photons are given in Ref. [50]. The large experimental effort ongoing at several electron accelerators to study the baryon resonance spectrum with real and virtual photon-induced meson production reactions includes the search for as-yet-unobserved states, as well as detailed studies of the properties of the low lying states (decay patterns, electromagnetic couplings, magnetic moments, *etc.*) (see Ref. [53] for reviews). There are two major new aspects of this program. The investigation of single and double polarization observables allows, via the study of interference terms, access to small partial waves that do not leave a footprint in unpolarized cross sections. An example for the impact of such data is given by a comparison of results from different multipole analyses of pion photoproduction [54]. It shows clearly that with the inclusion of polarization observables the reaction model results start to converge. This will in the near future

much improve the data basis for excited baryons in the light quark sector.

The other aspect is the study of final states with meson pairs, in particular $\pi\pi$ and $\pi\eta$ pairs, which made large progress during the last few years. This is important for higher lying states, which in the quark model may have both possible oscillations excited. Such states can be expected to decay in sequential processes de-exciting the two oscillations step-by-step so that they couple strongly to multiple-meson final states but not to single-meson production. Detailed analyses of such data are for example given in [55, 56] and had already significant impact on partial wave analyses.

The excitation spectrum of hyperons containing s-quarks is even less well explored. Many experimental results date back to before 2000, although parameters listed in the review are in many cases updated by more modern partial wave analyses. A recent review on the quark model interpretation of the Λ and Σ states is given in Ref. [57], a new Ω^- state was reported with high significance from the Belle experiment [58]. In the near future significant progress is expected from the PANDA experiment at FAIR [59, 60].

In quark models, the number of excited states is determined by the effective degrees of freedom, while their ordering and decay properties are related to the residual quark - quark interaction. An overview of quark models for baryons is given in [61], recent discussions of baryon spectroscopy are given in [45, 62]. The effective degrees of freedom in the standard nonrelativistic quark model are three equivalent valence quarks with one-gluon exchange-motivated, flavor-independent color-magnetic interactions. The QCD aspect of gluon-gluon interactions is emphasized by the hyper-central quark model [63, 64], which includes in a natural way three-body forces between the quarks. A different class of models uses interactions which give rise to a quark - diquark clustering of the baryons: for a review see [65]. If there is a tightly bound diquark, only two degrees of freedom are available at low energies, and thus *fewer* states are predicted. Furthermore, selection rules in the decay pattern may arise from the quantum numbers of the diquark. *More* states are predicted by collective models of the baryon like the algebraic approach in [66]. In this approach, the quantum numbers of the valence quarks are distributed over a Y-shaped string-like configuration, and additional states arise *e.g.*, from vibrations of the strings. *More* states are also predicted in the framework of flux-tube models, see [67], which are motivated by lattice QCD. In addition to the quark degrees of freedom, flux-tubes responsible for the confinement of the quarks are considered as degrees of freedom. These models include hybrid baryons containing explicit excitations of the gluon fields. However, since all half integral J^P quantum numbers are possible for ordinary baryons, such 'exotics' will be very hard to identify, and probably always mix with ordinary states. So far, the experimentally observed number of states is still far lower even than predicted by the quark–diquark models.

The influence of chiral symmetry on the excitation spectrum of the nucleon has been debated from a somewhat different perspective. Chiral symmetry, the fundamental symmetry of QCD, is strongly broken for the low lying states, resulting in large mass differences of parity partners like the $J^P{=}1/2^+$ $N(938)1/2^+$ ground state and the $J^P{=}1/2^-$ $N(1535)1/2^-$ excitation. However, at higher excitation energies there is some evidence for parity doublets and even some very tentative suggestions for full chiral multiplets of $N^\star$ and Δ resonances. An effective restoration of chiral symmetry at high excitation energies due to a decoupling from the quark condensate of the vacuum has been discussed (see Ref. [68] for recent reviews) as a possible cause. In this case, the mass generating mechanisms for low and high lying states would be essentially different. As a further consequence, the parity doublets would decouple from pions, so that experimental bias would be worse. However, parity doublets might also arise from the spin-orbital dynamics of the 3-quark system. Presently, the status of data does not allow final conclusions.

The most recent developments on the theory side are the first unquenched lattice calculations

for the excitation spectrum discussed in Sec. 15.8. The results are basically consistent with the level counting of SU(6)⊗O(3) in the standard non-relativistic quark model and show no indication for quark-diquark structures or parity doubling. Consequently, there is as yet no indication from lattice that the mis-match between the excitation spectrum predicted by the standard quark model and experimental observations is due to inappropriate degrees of freedom in the quark model.

15.5.2 *Charmed and bottom baryons*

The naming scheme for baryons with c or b quarks follows that of the light baryons: the Λ is an isosinglet and the Σ an isotriplet with one heavy (s, c or b) quark. The Ξ is an isodoublet which contains two heavy quarks, and the Ω an isosinglet with three heavy quarks. The number of c or b quarks is indicated by the subscripts c or b. Hyperons are baryons with at least one s quark.

For charmed baryons the addition of the c quark to the light quarks extends the flavor symmetry to $SU(4)_f$. Due to the large mass of the c quark, this symmetry is much more strongly broken than the $SU(3)_f$ of the three light quarks. Nevertheless, the $SU(4)_f$ representation is still useful for bookkeeping purposes. With the additive charm quantum number C the baryons are classified in a 3-dimensional representation with the three coordinates (I_z, Y , C). Figure 15.5 shows the $SU(4)_f$ weight diagrams.

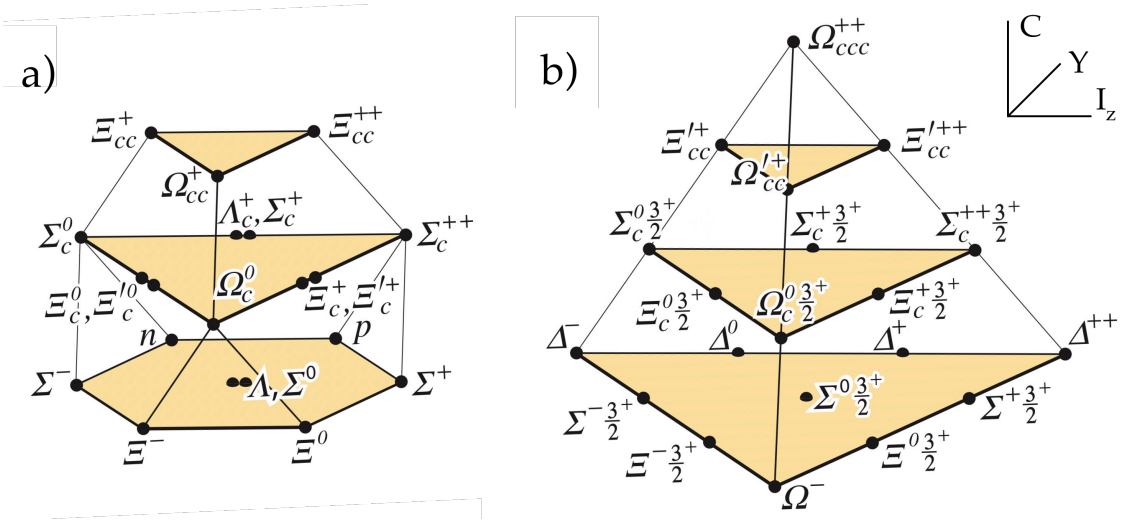

Figure 15.5: $SU(4)_f$ multiplets of ground state baryons made of u, d, s, and c quarks. (a) The spin $\frac{1}{2}$ 20-plet extends the charmless $SU(3)_f$ octet to C = 1,2; (b) the spin $\frac{3}{2}$ 20-plet extends the $SU(3)_f$ decuplet to C = 1, 2, 3.

With four quarks the 64 possible configurations decompose into

$$\mathbf{4} \otimes \mathbf{4} \otimes \mathbf{4} \otimes \mathbf{4} = \bar{\mathbf{4}}_A \oplus \mathbf{20}_S \oplus \mathbf{20}_{MS} \oplus \mathbf{20}_{MA}, \tag{15.29}$$

(for a review on $SU(N)$ symmetries see *e.g.* [69]). The subscripts S and A refer to the symmetry and antisymmetry properties of the flavor wave functions. The flavor symmetric 20_S multiplet, associated with spin-$\frac{3}{2}$ baryons, contains the charmless $SU(3)_f$ decuplet at the bottom level. The 20_{MS} and 20_{MA} multiplets correspond to the mixed symmetric and mixed antisymmetric flavour wave functions of the spin-$\frac{1}{2}$ baryons, with the charmless octet baryons at the bottom level. There are two dsc and two usc spin-$\frac{1}{2}$ states, labeled Ξ_c^0, $\Xi_c'^{\,0}$ and Ξ_c^+, $\Xi_c'^+$. This is because one of the qq pairs can have spin 1 (symmetric) or spin 0 (antisymmetric), giving both the total spin $j = \frac{1}{2}$ with the third quark (see also Fig. 15.6 below).

For $\mathsf{C} = 1$ baryons the flavor decomposition of the diquark, made of u, d, or s quarks, is

$$\mathbf{3} \otimes \mathbf{3} = \bar{\mathbf{3}}_A \oplus \mathbf{6}_S. \tag{15.30}$$

For ground-state baryons, the overall antisymmetry of baryon wave function (including color) requires the light diquark to be symmetric under the exchange of spin and flavor, hence both symmetric or both antisymmetric, that is spin 1 for the $\mathbf{6}_S$ and spin 0 for the $\bar{\mathbf{3}}_A$. The $\bar{\mathbf{3}}$ then combines with the c quark to form the $J^P = 1/2^+$ states, while the $\mathbf{6}$ combines to form $J^P = 1/2^+$ or $J^P = 3/2^+$. The weight diagrams of the $\bar{\mathbf{3}}$ and $\mathbf{6}$ ground-state representations are shown in Fig. 15.6. Within each multiplet the $\mathsf{C} = 1$ baryons obey isospin and $\mathrm{SU}(3)_f$ mass relations at the expected orders.

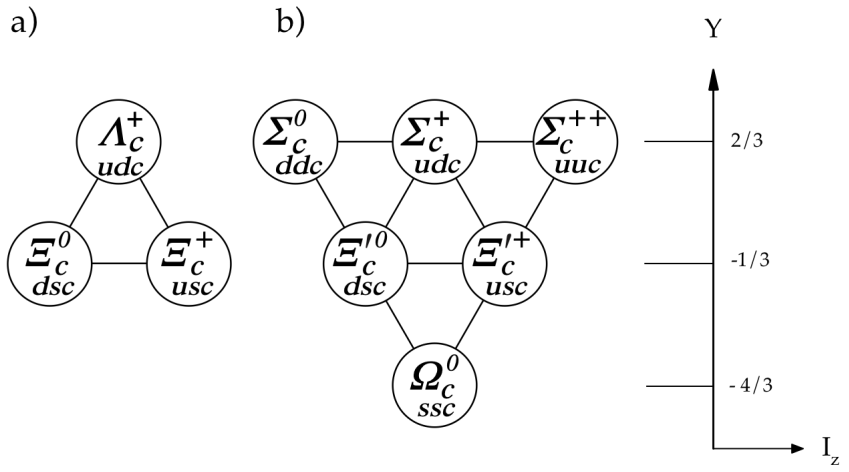

Figure 15.6: The $\mathrm{SU}(3)_f$ $\bar{\mathbf{3}}$ (a) and $\mathbf{6}$ (b) ground state $J^P = 1/2^+$ representations. The structure of the $\mathbf{6}$ ground state with $J^P = 3/2^+$ is identical to the one in (b).

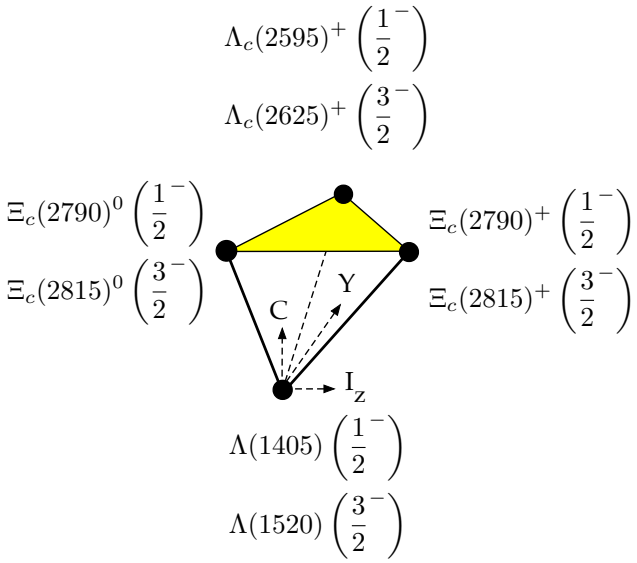

Figure 15.7: Weight diagram of the $\bar{\mathbf{4}}$ $\mathrm{SU}(4)_f$ multiplet with the experimentally observed negative parity baryons.

The antisymmetric quadruplet in (15.29) does not exist in the ground state but is realized for the first orbital excitations ($L = 1$). Figure 15.7 shows the weight diagram with the experimentally observed states. In the quark model the quadruplet consists of four baryons with spins coupling to $\frac{1}{2}$, leading to four $L = 1$ excitations with $J^P = \frac{1}{2}^-$ and four excitations with $\frac{3}{2}^-$. The charmed ones are the partners of the $\Lambda(1405)$ and $\Lambda(1520)$ singlets of $\mathrm{SU}(3)_f$.

For a detailed review on charmed baryons see Ref. [62]. Quark model predictions for baryons with two heavy quarks are given in Ref. [70] and lattice results for doubly and triply charmed states are discussed in Sec. 15.8 of this *Review*.

The $\mathsf{C} = 1$ ground state baryons have all been observed. Due to their relatively narrow widths the states are much easier to isolate than the light quark baryon resonances which require intricate partial wave analyses. The production cross sections are small, but the recent measurements at the e^+e^- B-factories, at the $p\bar{p}$ Tevatron collider, and at LHCb have boosted the field. The LHCb collaboration has published evidence for five new narrow Ω_c^0 states (css) [71] in proton-proton collisions. Four of these states have been confirmed by the Belle experiment in e^+e^- collisions [72]. Their quantum numbers are still unknown, but they could correspond to the $L = 1$ ssc orbital excitations. Constituent quark models, lattice QCD, quark-diquark models, molecular models, and pentaquark states, have been discussed to describe their structure (see e.g. [73] for references). In the meantime, also four Ω_b^- states of the bss type have been reported from LHCb [73]. They lie in a narrow range between 6316 - 6350 MeV, but since their intrinsic widths are on the order of just a few MeV they are well separated in the invariant mass spectra. Spectroscopy and theory in this field is rapidly evolving.

LHCb has also reported a doubly charmed Ξ_{cc}^{++} (ccu) baryon [74]. The quantum numbers of this state are undetermined, but its significance is already rated three stars in the current compilation. Doubly charmed baryons have a very different structure from light baryons, more resembling heavy 'double-star' systems with attached light 'planets', which opens a new window for QCD properties. The first candidate for a doubly charmed baryon Ξ_{cc}^{+} (ccd) had been reported earlier by the SELEX experiment [75, 76]. A significance of 6.3σ was claimed for the $\Lambda_c^+ K^- \pi^+$ decay and 4.8σ for pD^+K- but searches by other experiments have not confimed it so far (see *e.g.* [77] and Refs. therein) and it is not included in the particle listings. The SELEX and LHCb masses lie in the predicted 3500 – 3700 MeV mass range (see *e.g.* [70]). The LHCb Ξ_{cc}^{++} state lies about 100 MeV above the SELEX one, with a mass splitting far too large for ucc and dcc isospin partners. However, it has also been discussed that due to the different production mechanisms this is not necessarily a contradiction [78].

Figure 15.8 shows the spectrum of the established singly-charmed baryons (3* and 4* baryons in the *Listings* with known quantum numbers). The parity of the Λ_c^+ is that of the c quark, defined as positive. Spin and parity have not been determined experimentally for most of the states. They follow the ordering and expectation from the quark model. Candidates for $L = 2$ orbital excitations of the Λ_c (with $J^P = \frac{3}{2}^+$ and $J^P = \frac{5}{2}^+$) have already been observed, as well as a $\frac{3}{2}^-$ state at 2940 MeV, possibly a radial $L = 1$ excitation [79].

The same $\mathrm{SU}(4)_f$ multiplets can be constructed for the bottom baryons by replacing the c quark by a b quark.The established 3* and 4* bottom baryons are shown in Fig.15.8. The quadruplet $\bar{\mathbf{4}}$ contains the two negative parity candidates $\Lambda_b(5912)^0$ and $\Lambda_b(5920)^0$. It appears that the confining potential is only weakly flavour dependent. For example, the mass difference between the Ξ_b and the Λ_b is roughly the same as that between the Ξ_c and the Λ_c, the mass splitting between the spin-$\frac{1}{2}$ Ω_b and the Λ_b close to that between the spin-$\frac{1}{2}$ Ω_c and the Λ_c. The spin-$\frac{3}{2}$ states are also heavier than the spin-$\frac{1}{2}$ ones, in agreement with expectations from the spin-spin force.

The bottom hadrons can also be embedded in a larger $\mathrm{SU}(5)_f$ group that accounts for all baryons constructed from the five quark flavors. (The existence of baryons with t-quarks is very

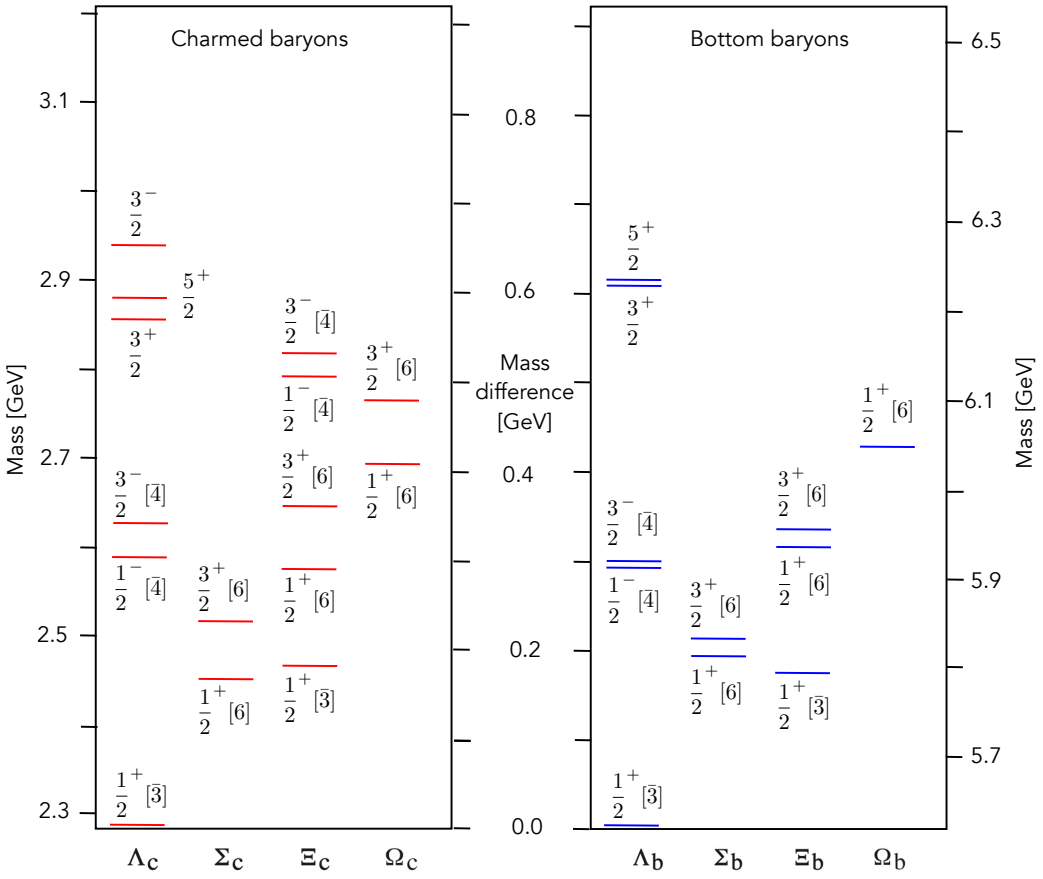

Figure 15.8: Mass spectrum of the established C = 1 charmed and B = –1 bottom baryons with known J^P. The flavor symmetry assignments are given by the square brackets. According to their isospins the $\Sigma_{c,b}$ ($\Xi_{c,b}$) consist of three (two) charged or neutral states that are nearly degenerate.

unlikely due to the short lifetime of the t-quark.) One predicts the decomposition

$$\mathbf{5} \otimes \mathbf{5} \otimes \mathbf{5} = \overline{\mathbf{10}}_A \oplus \mathbf{40}_{MS} \oplus \mathbf{40}_{MA} \oplus \mathbf{35}_S. \tag{15.31}$$

The decuplet is not realized in the ground state. The two 40-plets have mixed symmetry ($\frac{1}{2}$-spin) and the 35-plet is symmetric ($\frac{3}{2}$-spin). The SU(4)$_f$ spin-$\frac{1}{2}$ multiplet in Fig. 15.5 contains 20 spin-$\frac{1}{2}$ baryons and the corresponding one with bottom quarks an additional 12, giving together 32 states. Similarly there are 30 spin-$\frac{3}{2}$ baryons. One expects 75 ground state mesons from (15.31). Thus 13 ground state baryons containing both b and c quarks are predicted (8 spin-$\frac{1}{2}$ [$4\Omega + 4\Xi$] and 5 spin-$\frac{3}{2}$ [$3\Omega + 2\Xi$]).

15.6 Magnetic moments

The magnetic dipole moment of a baryon is conventionally written relative to the mass of the proton:

$$\vec{\mu}_B = g_B \mu_N \vec{s}, \tag{15.32}$$

where $\mu_N = \frac{e}{2m_p}$ is the nuclear magneton (in natural units). The factor g_B is calculated by adding the quark contributions. The magnetic moment of quark i with charge $q_i e$ and constituent mass m_i is $\vec{\mu}_i = 2(\frac{q_i e}{2m_i})\vec{s}$, hence for the three light quarks,

$$\mu_u = \frac{2}{3}\kappa_u, \quad \mu_d = -\frac{1}{3}\kappa_d, \quad \mu_s = -\frac{1}{3}\kappa_s, \quad \text{with} \quad \kappa_i \equiv \frac{e}{2m_i}. \tag{15.33}$$

The magnetic dipole moment of a baryon is then given by

$$\mu_B = \sum_{i=1}^{3} \langle B \uparrow | \mu_i \sigma_{zi} | B \uparrow \rangle, \tag{15.34}$$

where $|B \uparrow\rangle$ is the wavefunction for a baryon with its spin along the z-axis and $\vec{\sigma} = 2\vec{s}$. Since the quark model uses the totally *symmetric* SU(6) wavefunctions (flavor SU(3) $\times$ spin SU(2)) one predicts for the proton:

$$\mu_p = \frac{4}{3}\mu_u - \frac{1}{3}\mu_d = \frac{e}{2m} \equiv \kappa, \tag{15.35}$$

assuming $m_u = m_d \simeq m$ (for the detailed derivation see *e.g.* Ref. [4]). For the magnetic moment of the neutron one obtains likewise

$$\mu_n = -\frac{1}{3}\mu_u + \frac{4}{3}\mu_d = -\frac{2}{3}\kappa, \tag{15.36}$$

which leads to the simple prediction $\mu_n/\mu_p = g_n/g_p = -2/3$.

The famous Frisch and Stern experiment showed for the first time that $g_p \sim 5.58 \gg 2$. Modern measurements are performed in electromagnetic traps, see the *Listings*, while the magnetic moment of the neutron is measured with cold neutron beams. The experimental ratio $\mu_n/\mu_p = -0.6849793 \pm 0.0000003$ is impressively close to the prediction of the quark model (note that using instead the *antisymmetric* SU(6) wavefunctions would lead to $\mu_n/\mu_p = -2$ [4]). The constituent mass m of the u and d quarks can be estimated from (15.32) and (15.35): $m = 2m_p/g_p \simeq 336$ MeV.

The magnetic moment of the Λ is easy to predict: the diquark ud has isospin $i = 0$, since $i(s) = 0$ and $i(\Lambda) = 0$, and is therefore an antisymmetric isospin state. The symmetric quark model then also requires the spin to be zero, so that the magnetic moment of the Λ stems from the s quark:

$$\mu_\Lambda = \mu_s = -\frac{1}{3}\kappa_s. \tag{15.37}$$

The magnetic moment of the Λ is obtained from the Larmor precession frequency of the polarization vector in an homogeneous magnetic field. The latter is derived from the asymmetric distribution of the proton in $\Lambda \to \pi^- p$ [80]. The experimental result is listed in Table 15.8. The constituent mass of the s quark is then $m_s = -m\mu_p/3\mu_\Lambda = 509$ MeV.

The magnetic moments of the other baryons (Table 15.8) are predicted from κ and κ_s. The magnetic moment of the Σ^+ is obtained by replacing the d quark in (15.35) by an s quark, and for the Σ^- the u quark by an s quark in (15.36). The magnetic moment of the Σ^+ has also been measured with the precession method using its decay into $p\pi^0$ [81], that of the $\Sigma^- \to n\pi^-$ likewise, or by detecting the X-rays emitted by cascading Σ^- captured in the Coulomb shells of target atoms. The magnetic moment is then derived from the fine-structure splitting [82].

The magnetic moments of the Ξ^0, Ξ^- and Ω^- are obtained from the polarization of the Λ in the decays $\Lambda\pi^0$, $\Lambda\pi^-$ and ΛK^-, respectively. The SU(6) wavefunction of the (spin 3/2) Ω^- is the product of the two symmetric SU(3) flavor and SU(2) spin wavefunctions. Summing over the three s quarks one gets

$$\mu_{\Omega^-} = \sum_{i=1}^{3} \langle \Omega^- \uparrow | \mu_i \sigma_{zi} | \Omega^- \uparrow \rangle = 3\mu_s = 3\mu_\Lambda. \tag{15.38}$$

The magnetic moment of the Ω^- is hard to measure, because the Ω^- is unpolarized at high energies, in contrast to the other hyperons. Polarized Ω^- hyperons have been obtained from polarized Λ and Ξ^0 impinging on a nuclear target [83].

Table 15.8: Quark model predictions and measured magnetic dipole moments of the ground state baryons in units of μ_N; $\kappa \equiv \frac{e}{2m} = 2.793\ \mu_N$ and $\kappa_s \equiv \frac{e}{2m_s} = -3\mu_\Lambda = 1.84\ \mu_N$. $^\dagger\Sigma^0 \to \Lambda$ transition magnetic moment.

Baryon	Quark model			Experimental value		
p	κ		input	2.793		
n	$-\frac{2}{3}\kappa$	=	–1.86	–1.913		
Λ	$-\frac{1}{3}\kappa_s$		input	–0.6138	±	0.0047
Σ^+	$\frac{8}{9}\kappa + \frac{1}{9}\kappa_s$	=	2.68	2.458	±	0.010
Σ^0	$\frac{2}{9}\kappa + \frac{1}{9}\kappa_s$	=	0.82			
$\Sigma^{0\dagger}$	$-\frac{1}{\sqrt{3}}\kappa$	=	–1.61	–1.61	±	0.08
Σ^-	$-\frac{4}{9}\kappa + \frac{1}{9}\kappa_s$	=	–1.04	–1.160	±	0.025
Ξ^0	$-\frac{2}{9}\kappa - \frac{4}{9}\kappa_s$	=	–1.44	–1.250	±	0.014
Ξ^-	$\frac{1}{9}\kappa - \frac{4}{9}\kappa_s$	=	–0.51	–0.6507	±	0.0025
Ω^-	$-\kappa_s$	=	–1.84	–2.024	±	0.056
Δ^{++}	2κ	=	5.58	4.52	±	0.67
Δ^+	κ	=	2.79	2.3	-	4.5

In quark models with full isospin symmetry the magnetic moments of the Δ-resonances are simply related to the magnetic moment of the proton by $\mu_\Delta = Q_\Delta \cdot \mu_N$, ($Q_\Delta$ = charge) i.e. the moment of the Δ^+ should equal the proton moment and the moment of the Δ^{++} should be twice as large (sum of the three u-quarks). Magnetic moments of the decuplet baryons (with the exception of the Ω^-) are very difficult to measure because their lifetimes are so short that spin precession techniques cannot be used. For the Δ one can profit from an electromagnetic spin-reorientation transition inside the large width of the state. This leads to the emission of a magnetic dipole photon in reactions like $\pi^+ p \to \pi^+ p\gamma$ or $\gamma p \to \pi^0 p\gamma'$ which is related to the magnetic moment of the resonance. The first reaction has been used to study the magnetic moment of the Δ^{++} by measuring the left-right asymmetry with polarized protons [84]. The second one was used for the Δ^+ state [85, 86]. Taking all experimental and systematic uncertainties into account the result spans the range from (2.3 - 4.5)μ_N, covering the quark model prediction of ≈2.8μ_N, but is not very precise.

Table 15.8 lists the current experimental values for the magnetic moments of the ground state baryons, together with the predictions from the quark model. There are significant discrepancies, but given its crudeness, the quark model performs surprisingly well.

15.7 Dynamics

Quantum chromodynamics (QCD) is well-established as the theory for the strong interactions. As such, one of the goals of QCD is to predict the spectrum of strongly-interacting particles. To date, the only first-principles calculations of spectroscopy from QCD use lattice methods. These are the subject of Sec. 15.8. These calculations are difficult and unwieldy, and many interesting questions do not have a good lattice-based method of solution. Therefore, it is natural to build models, whose ingredients are abstracted from QCD, or from the low-energy limit of QCD (such as chiral Lagrangians) or from the data itself. The words "quark model" are a shorthand for such phenomenological models. Many specific quark models exist, but most contain a similar basic set of dynamical ingredients. These include:

1. A confining interaction, which is generally spin-independent (*e.g.*, harmonic oscillator or linear confinement);
2. Different types of spin-dependent interactions:

   a) commonly used is a color-magnetic flavor-independent interaction modeled after the effects of gluon exchange in QCD (see *e.g.*, Ref. [87]). For example, in the S-wave states, there is a spin-spin hyperfine interaction of the form

   $$H_{HF} = -\alpha_S M \sum_{i>j} (\vec{\sigma}\lambda_a)_i (\vec{\sigma}\lambda_a)_j, \tag{15.39}$$

   where M is a constant with units of energy, λ_a $(a = 1, \cdots, 8,)$ is the set of SU(3) unitary spin matrices, defined in the review "SU(3) Isoscalar Factors and Representation Matrices," and the sum runs over constituent quarks or antiquarks. Spin-orbit interactions, although allowed, seem to be small in general, but a tensor term is responsible for the mixing of states with the same J^P but different L, S combinations.

   b) other approaches include flavor-dependent short-range quark forces from instanton effects (see *e.g.*, [88, 89]). This interaction acts only on scalar, isoscalar pairs of quarks in a relative S-wave state:

   $$\langle q^2; S, L, T|W|q^2; S, L, T\rangle = -4g\delta_{S,0}\delta_{L,0}\delta_{I,0}\mathcal{W} \tag{15.40}$$

   where $\mathcal{W}$ is the radial matrix element of the contact interaction.

   c) a rather different and somewhat controversial approach is based on flavor-dependent spin-spin forces arising from one-boson exchange. The interaction term is of the form:

   $$H_{HF} \propto \sum_{i<j} V(\vec{r}_{ij}) \lambda_i^F \cdot \lambda_j^F \vec{\sigma}_i \cdot \vec{\sigma}_j \tag{15.41}$$

   where the λ_i^F are in flavor space (see *e.g.*, Ref. [90]).
3. A strange quark mass somewhat larger than the up and down quark masses, in order to split the SU(3) multiplets;
4. In the case of spin-spin interactions, a flavor-symmetric interaction for mixing $q\bar{q}$ configurations of different flavors (*e.g.*, $u\bar{u} \leftrightarrow d\bar{d} \leftrightarrow s\bar{s}$), in isoscalar channels, so as to reproduce *e.g.*, the η - η' and ω - ϕ mesons.

These ingredients provide the basic mechanisms that determine the hadron spectrum in the standard quark model.

15.8 Lattice Calculations of Hadronic Spectroscopy

Lattice calculations are a major source of information about QCD masses and matrix elements. The necessary theoretical background is given in Sec. 17 of this *Review*. Here we confine ourselves to some general comments and illustrations of lattice calculations for spectroscopy.

It might seem a bit out of place to have a section about lattice calculations in a review of the quark model, since to many readers, the quark model is just a model while QCD could be thought of as a construct which is something deeper than a model. But this review is, despite its title, actually an introduction to the spectroscopy and related quantities of the strong interactions. From that perspective, a presentation of lattice results is entirely appropriate.

Lattice calculations are from first principles – their input is a discretized version of the QCD Lagrangian, and the predictions of a lattice calculation are predictions of QCD, once the lattice

spacing is taken to zero, the simulation volume is taken to infinity, and the quark masses are tuned to their physical values. Lattice calculations make extensive use of quark model ideas – for example, the operators used to create and annihilate hadrons are almost always based on the quark model. (This may not be clear in the lattice literature, since the final answer should not depend on the choice of operators used.)

There is only a sporadic literature connecting lattice results to the quark model (one recent example is [91]) but of course the qualitative understanding of lattice results depends as heavily on quark model ideas as does the qualitative understanding of experimental data.

In general, the cleanest lattice results come from computations of processes in which there is only one particle in the simulation volume. These quantities include masses of hadrons, simple decay constants, like pseudoscalar meson decay constants, and semileptonic form factors (such as the ones appropriate to $B \to Dl\nu$, $Kl\nu$, $\pi l\nu$). The cleanest predictions for masses are for states which have narrow decay widths and are far below any thresholds to open channels, since the effects of final state interactions are not yet under complete control on the lattice. As a simple corollary, the lightest state in a channel is easier to study than the heavier ones. "Difficult" states for the quark model (such as exotics) are also difficult for the lattice because of the lack of simple operators which couple well to them.

Good-quality modern lattice calculations will present multi-part error budgets with their predictions. A small part of the uncertainty is statistical, from sample size. Typically, the quoted statistical uncertainty includes uncertainty from a fit: it is rare that a simulation computes one global quantity which is the desired observable. Simulations which include virtual quark-antiquark pairs (also known as "dynamical quarks" or "sea quarks") are often done at up and down quark mass values heavier than the experimental ones, and it is then necessary to extrapolate in these quark masses. Simulations can work at the physical values of the heavier quarks' masses. They are always done at nonzero lattice spacing, and so it is necessary to extrapolate to zero lattice spacing. Some theoretical input is needed to do this. Much of the uncertainty in these extrapolations is systematic, from the choice of fitting function. Other systematics include the effect of finite simulation volume, the number of flavors of dynamical quarks actually simulated, and technical issues with how these dynamical quarks are included. The particular choice of a fiducial mass (to normalize other predictions) is not standardized; there are many possible choices, each with its own set of strengths and weaknesses, and determining it usually requires a second lattice simulation from that used to calculate the quantity under consideration.

A systematic error of major historical interest is the "quenched approximation," in which dynamical quarks are simply left out of the simulation. This was done because the addition of these virtual pairs presented an expensive computational problem. No generally-accepted methodology has ever allowed one to correct for quenching effects, short of redoing all calculations with dynamical quarks. Recent advances in algorithms and computer hardware have rendered it obsolete.

With these brief remarks, we turn to examples. The field of lattice QCD simulations is vast, and so it is not possible to give a comprehensive review of them in a small space. The history of lattice QCD simulations is a story of thirty years of incremental improvements in physical understanding, algorithm development, and ever faster computers, which have combined to bring the field to a present state where it is possible to carry out very high quality calculations. We present a few representative illustrations, to show the current state of the art.

15.8.1 *Spectroscopy of low-lying states*

By far, the major part of all lattice spectroscopy is concerned with that of the light hadrons, and so we illustrate results in Fig. 15.9, a comprehensive summary provided by A. Kronfeld (private communication; see also [105]).

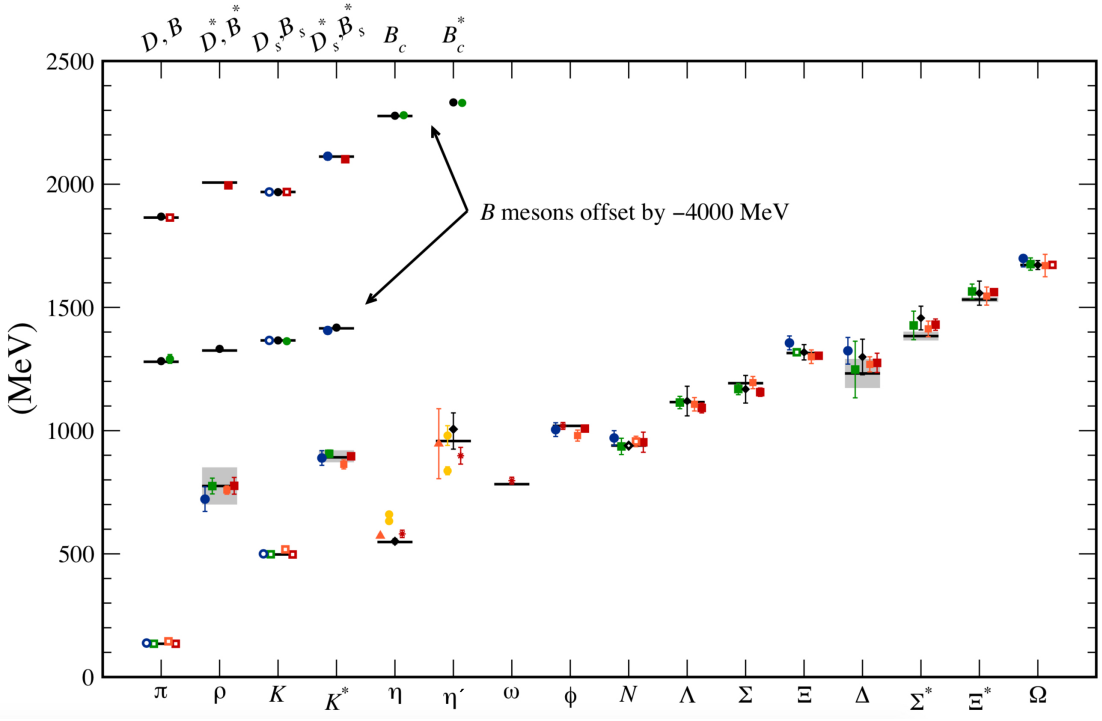

Figure 15.9: Hadron spectrum from lattice QCD. Comprehensive results for mesons and baryons are from MILC [92, 93], PACS-CS [94], BMW [95], QCDSF [96], and ETM [97]. Results for η and η' are from RBC & UKQCD [17], Hadron Spectrum [98] (also the only ω mass), UKQCD [99], and Michael, Ottnad, and Urbach [100]. Results for heavy-light hadrons from Fermilab-MILC [101], HPQCD [102, 103], and Mohler and Woloshyn [104]. Circles, squares, diamonds, and triangles stand for staggered, Wilson, twisted-mass Wilson, and chiral sea quarks, respectively. Asterisks represent anisotropic lattices. Open symbols denote the masses used to fix parameters. Filled symbols (and asterisks) denote results. Red, orange, yellow, green, and blue stand for increasing numbers of ensembles (i.e., lattice spacing and sea quark mass) Black symbols stand for results with 2+1+1 flavors of sea quarks. Horizontal bars (gray boxes) denote experimentally measured masses (widths). b-flavored meson masses are offset by -4000 MeV.

Mesons with a valence structure of identical quark - antiquark pairs such as the eta or eta-prime, $|\eta\rangle \sim \alpha|\bar{u}u + \bar{d}d\rangle + \beta|\bar{s}s\rangle$, are at the frontier of lattice QCD calculations, because one must include the effects of "annihilation graphs" for the valence q and $\bar{q}$. Recently, several groups, Refs. [17, 99, 106], have reported calculations of the η and η' mesons. The numbers of [17] are typical, finding masses of 573(6) and 947(142) MeV for the η and η'. The singlet-octet mixing angle (in the conventions of Table 15.2) is $\theta_{lin} = -14.1(2.8)^\circ$.

The spectroscopy of mesons containing heavy quarks has become a truly high-precision endeavor. These simulations use Non-Relativistic QCD (NRQCD) or Heavy Quark Effective Theory (HQET), systematic expansions of the QCD Lagrangian in powers of the heavy quark velocity, or the heavy quark mass. Terms in the Lagrangian have obvious quark model analogs, but are derived directly from QCD. For example, the heavy quark potential is a derived quantity, extracted from simulations. Figs. 15.10 and 15.11 show the low lying mass spectrum for charmonium and bottomonium states from two different groups [103, 107]. Most of the results are for the lightest state with a given value of quantum numbers. We return to this point below.

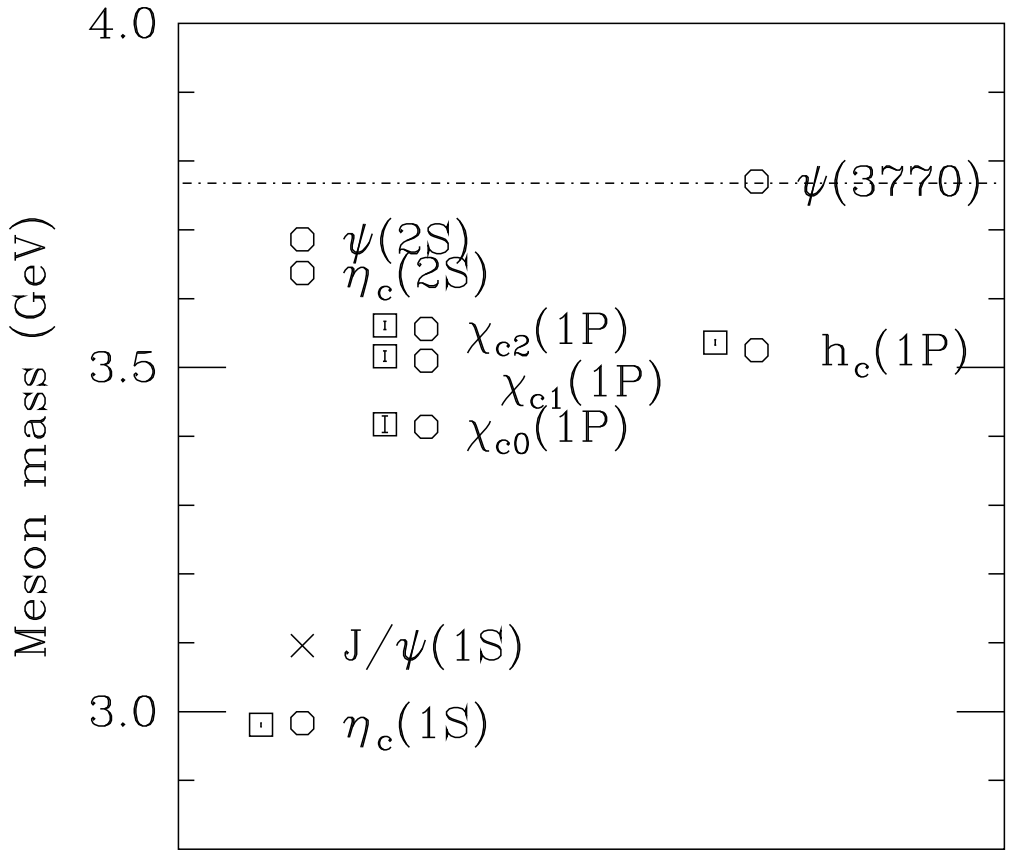

Figure 15.10: Spectroscopy of the $\bar{c}c$ spectrum, compared to lattice data from Ref. [107]. Particles whose masses are used to fix lattice parameters are shown with crosses; octagons label experimental values, and lattice results are shown as squares. The dotted line shows the threshold value for two charmed mesons.

Fig. 15.12 shows a compilation of recent lattice results for doubly and triply charmed baryons, provided by S. Meinel [115]. The state recently announced by LHCb [74] is also shown. Note that the lattice calculations for the mass of this state were predictions, not postdictions.

15.8.2 *Excited state spectroscopy*

Lattice calculations of excited states are much more difficult than those for the lightest states. There are two issues:

1. The states are unstable resonances
2. There are many states with the same quantum numbers

While these two problems appear together in excited state spectroscopy, almost all lattice calculations we know of deal with them separately (i. e. there are studies of many stable states, or studies of a single state with a single decay channel).

The first point is an issue because lattice calculations do not see decays directly; instead, they give energies of single or multiple particle states in a box of finite size. The combined mass is shifted from being the sum of the individual masses because the finite box size forces the hadrons to interact with each other. The volume-dependent mass shift yields the phase shift for the continuum scattering amplitude, which in turn can be used to extract the resonance mass and width, with some degree of modeling. So far only two-body resonances, the rho meson and a few others, have

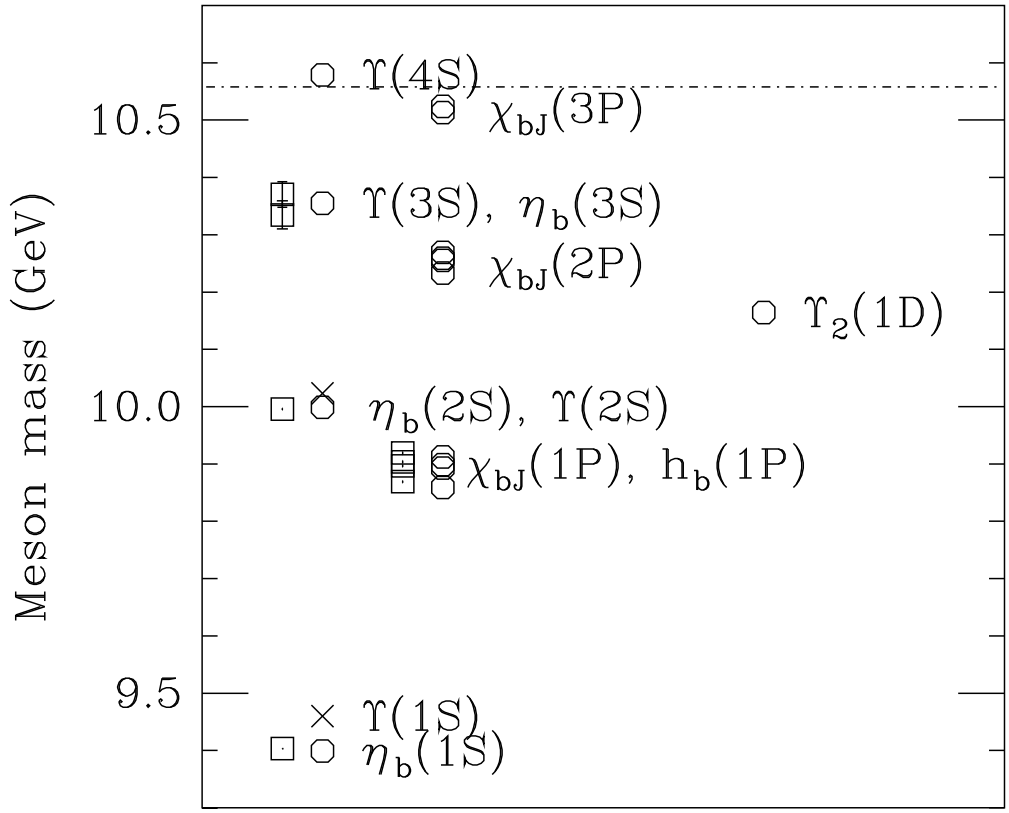

Figure 15.11: Spectroscopy of the $\bar{b}b$ system, adapted from Ref. [103]. Particles whose masses are used to fix lattice parameters are shown with crosses; octagons label experimental values, and lattice results are shown as squares. The dotted line shows the threshold value for two bottom mesons.

been well studied. This is an active research area. A recent review, [116], summarizes the situation, and example of a calculation of the rho meson decay width is [117]. The mass and decay width of the $f_0(500)$ have recently been computed in [118] and [119]. Ref. [120] studies the decay width of the $\Delta(1238)$.

The second point is an issue for lattice calculations since the observables which give masses have a typical functional form

$$C(t) = \sum_n A_n \exp(-E_n t). \tag{15.42}$$

E_n is the energy of the nth state and t is a parameter (the spatial distance of separation of operators) which is accessible to the lattice simulator. The contribution of excited states is exponentially suppressed at large t. The size of a given state's contribution, A_n, is related to the choice of interpolating field use to create the state. (This is where the quark model comes in.) As we move away from hadrons which can be created by the simplest quark model operators (appropriate to the lightest meson and baryon multiplets) we encounter a host of new problems: either no good interpolating fields, or too many possible interpolating fields, and many states with the same quantum numbers. Techniques for dealing with these interrelated problems vary from collaboration to collaboration, but all share common features: typically, correlation functions from many different interpolating fields are used, and the signal is extracted in what amounts to a variational calculation using the chosen operator basis. In addition to mass spectra, wave function information can be

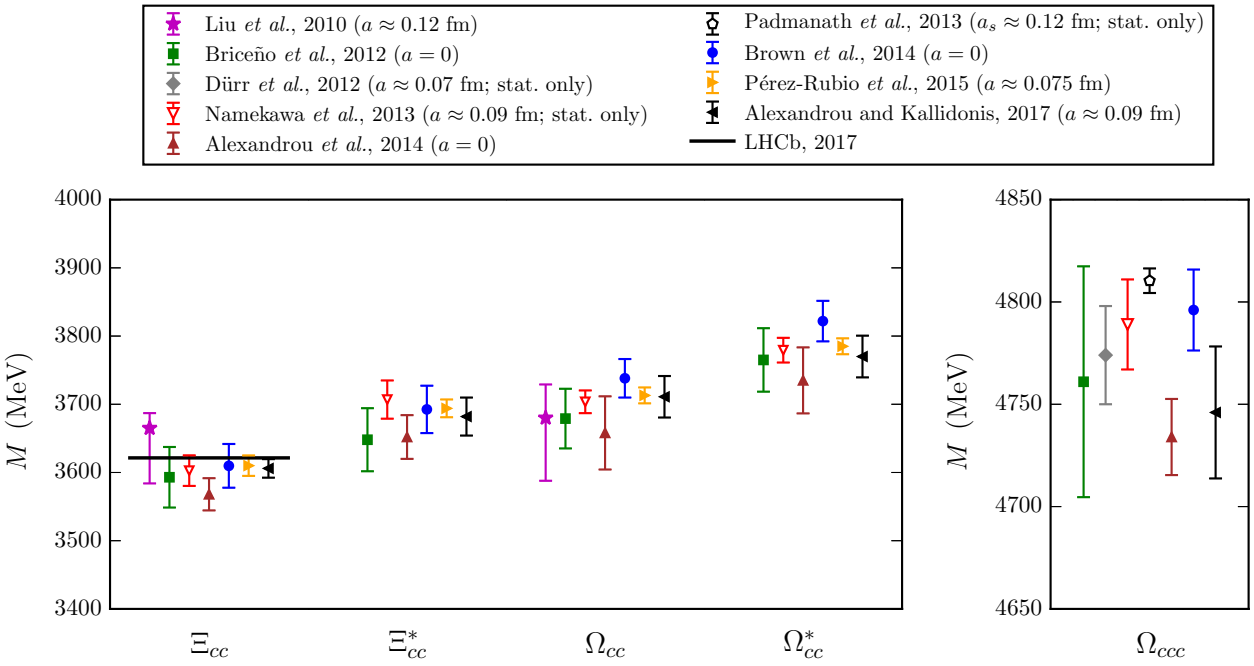

Figure 15.12: Comparison of lattice QCD results for the doubly and triply charmed baryon masses. Labels are Liu, *et al.*, [108]; Briceno, *et al.*, [109]; Namekawa, *et al.*, [110]; Padmanath, *et al.*, [111]; Alexandrou, *et al.*, [97]; Brown, *et al.*, [112]; Perez-Rubio *et al.*, [113]; Alexandrou and Kallidonis 2017, [114]. Only calculations with dynamical light quarks are included; for the doubly charmed baryons, only calculations were performed at or extrapolated to the physical pion mass are shown. Results without estimates of systematic uncertainties are labeled "stat. only". The lattice spacing values used in the calculations are also given; $a = 0$ indicates that the results have been extrapolated to the continuum limit. In the plot of the doubly charmed baryons, the recently announced experimental result for the Ξ_{cc}^{+} mass from LHCb [74] is shown with a horizontal line.

garnered from the form of the best variational wave function. Of course, the same problems which are present in the spectroscopy of the lightest hadrons (the need to extrapolate to infinite volume, physical values of the light quark masses, and zero lattice spacing) are also present. We briefly touch on three different kinds of hadrons: excited states of mesons (including hybrids), excited states of baryons, and glueballs. The quality of the data is not as good as for the ground states, and so the results continue to evolve. Shifts in the masses which occur because the state can decay are not included in the calculations.

Modern calculations use a large basis of trial states, which allow them to probe many quantum number channels simultaneously. This is vital for studying "difficult sectors" of QCD, such as the isoscalar mesons. A recent example of meson spectroscopy where this is done, by [121], is shown in Fig. 15.13. The quark masses are still heavier than their physical values, so the pion is at 392 MeV. The authors can assign a relative composition of nonstrange and strange quark content to their states, observing, for example, a nonstrange ω and a strange ϕ. Some states also have a substantial component of gluonic excitation. Note especially the three exotic channels $J^{PC} = 1^{-+}$, 0^{+-}, and 2^{+-}, with states around 2 GeV. These calculations will become more realistic as the quark masses are carried lower and resonance effects are included.

The interesting physics questions of excited baryon spectroscopy to be addressed are precisely those enumerated in the last section. An example of a recent calculation, due to Ref. [122] is shown

in Fig. 15.14. Notice that the pion is not yet at its physical value. The lightest positive parity state is the nucleon, and the Roper resonance has not yet appeared as a light state.

Studies which observe a large basis of states across many volumes can probe excited state spectroscopy as resonances. These calculations are just beginning and the ones we know about are performed at unphysically heavy quark masses. Examples include the decays of an exotic $J^{PC} = 1^{-+}$ resonance [123] and the spectroscopy of J^{--} resonances [124]. We expect to see considerable progress in this area over the next few years.

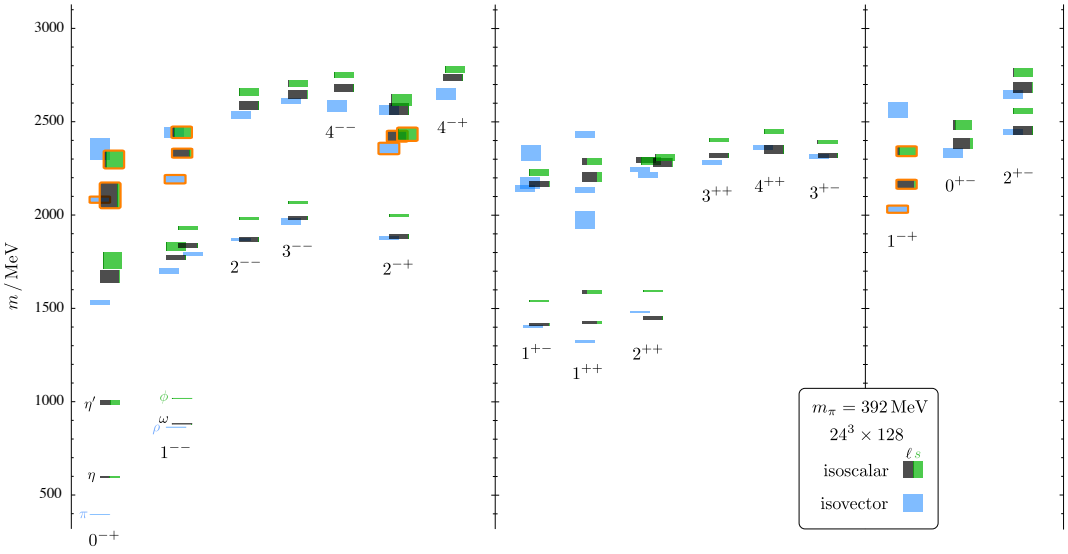

Figure 15.13: Isoscalar (green and black) and isovector (blue) spectrum from Ref. [121]. States are labeled J^{PC}. The quark mass is heavier than its physical value; $m_\pi = 392$ MeV. The vertical height of each box indicates the statistical uncertainty in the mass. Black and green indicate relative nonstrange and strange composition. Orange outlines show states with a large chromomagnetic component to their wave function, which the authors argue are hybrid states. Note the exotic states in the three rightmost columns.

Glueballs present similar issues. In Fig. 15.3 we showed a figure from [22] presenting a lattice prediction for the glueball mass spectrum in quenched approximation. A true QCD prediction of the glueball spectrum requires dynamical light quarks, some way to deal with the mixing of glue states and quark-antiquark (and beyond) states and (because glueball operators are intrinsically noisy) high statistics. Only recently have the first useful such calculations appeared, in [125, 126]. Fig. 15.15 shows results from [125], done with dynamical u, d and s quarks at two lattice spacings, 0.123 and 0.092 fm, along with comparisons to the quenched lattice calculation of [25] and to experimental isosinglet mesons. The dynamical simulation is, of course, not the last word on this subject, but it shows that the effects of quenching seem to be small.

Lattice calculations relevant to the extra states observed in the charmonium and bottomonium spectrum (Sec. 15.4) are difficult, because the states sit high in the spectrum of most channels, because of the number of nearby multiparticle states, and because it is necessary to have the technology to study heavy and light quarks together. There is a hybrid literature of studies which combines lattice calculations of the potential of static sources in a solution of a Schrödinger equation for the light quarks in a Born - Oppenheimer approximation (see [127] for context).

The system with the largest lattice literature is a bound state of two heavy quarks and two light antiquarks, for example $\bar{b}\bar{b}ud$. There are excellent reasons for expecting this state to be stable

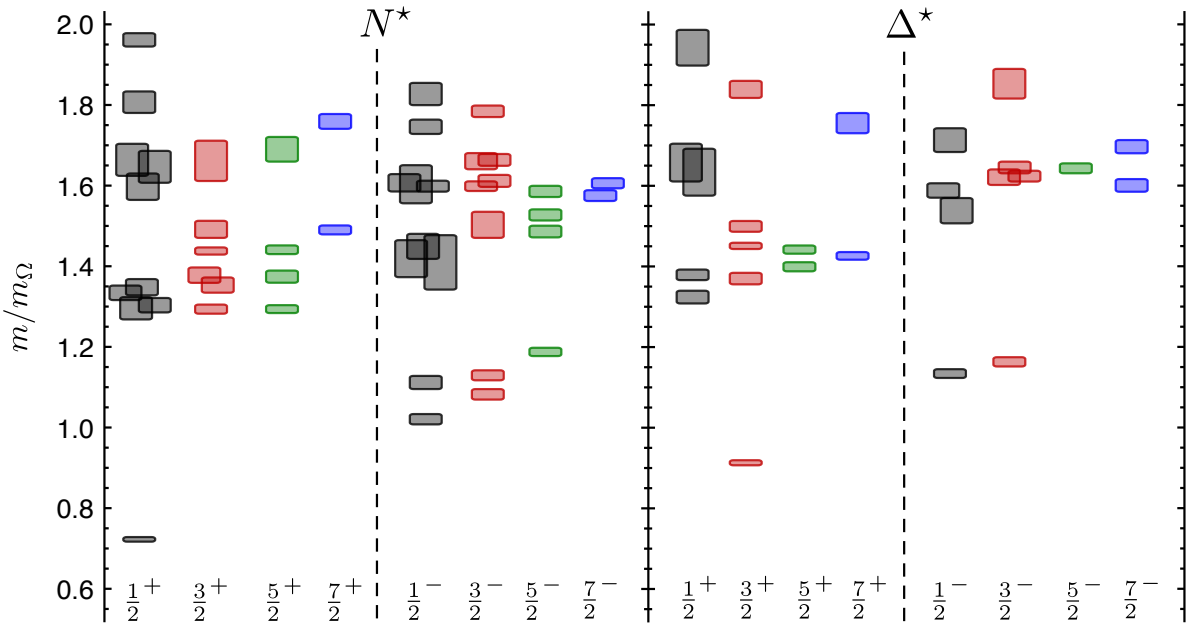

Figure 15.14: Spin-identified spectrum of nucleons and deltas, from lattices where $m_\pi = 396$ MeV, in units of the calculated Ω mass, from Ref. [122]. The colors just correspond to the different J assignments: grey for $J = 1/2$, red for $J = 3/2$, green for 5/2, blue for $J = 7/2$.

in the limit that the b mass goes to infinity [128] but finding the precise degree of stability at the physical b mass takes a phenomenological estimate or a lattice calculation. The $I(J^P) = 0(1^+)$ state is predicted to be stable by about 128(26) MeV [129] or 189(10) MeV [130]. (These authors put the $\bar{b}\bar{b}sd$ state at 98 MeV below threshold.) These numbers are in reasonable agreement with phenomenological estimates from Refs. [128, 131].

15.8.3 *Electromagnetic effects*

As a final part of spectroscopy we mention electromagnetic mass splittings (such as the neutron - proton mass difference). They are interesting but difficult. These calculations are important for determining the values of the quark masses (for a discussion see Sec. 60 in this Review). Knowing that the neutron is heavier than the proton tells us that these splittings have a complicated origin. One part of the shift is because the up and down quarks have slightly different masses. The second is that the quarks have (different) charges. Phenomenologists (compare Ref. [132]) combine Coulomb forces and spin-dependent electromagnetic hyperfine interactions to model their charge effects. In order to compute hadronic mass differences on the lattice, electromagnetic interactions must be included in the simulations. This creates a host of technical issues. An important one is that electromagnetic interactions are long range, but lattice simulations are done in finite volumes. The theoretical situation is summarized in the recent Flavour Lattice Averaging Group (FLAG) review [133]. A recent calculation, Ref. [134], has presented the first results for electromagnetic mass splittings in the baryon octet, with good agreement with observation. Refs. [135–137] have performed calculations for meson splittings.

There is a small lattice literature associated with magnetic moments of baryons. The calculations are done by including a static magnetic field in the simulation and computing the energy difference between baryons in different spin states. We are aware of no calculations at physical quark masses. A recent calculation [138] used 800 and 450 MeV pions. When expressed in units of the nucleon magneton at the simulation point ($e/(2M_N(m_\pi))$) the moments are in reasonable

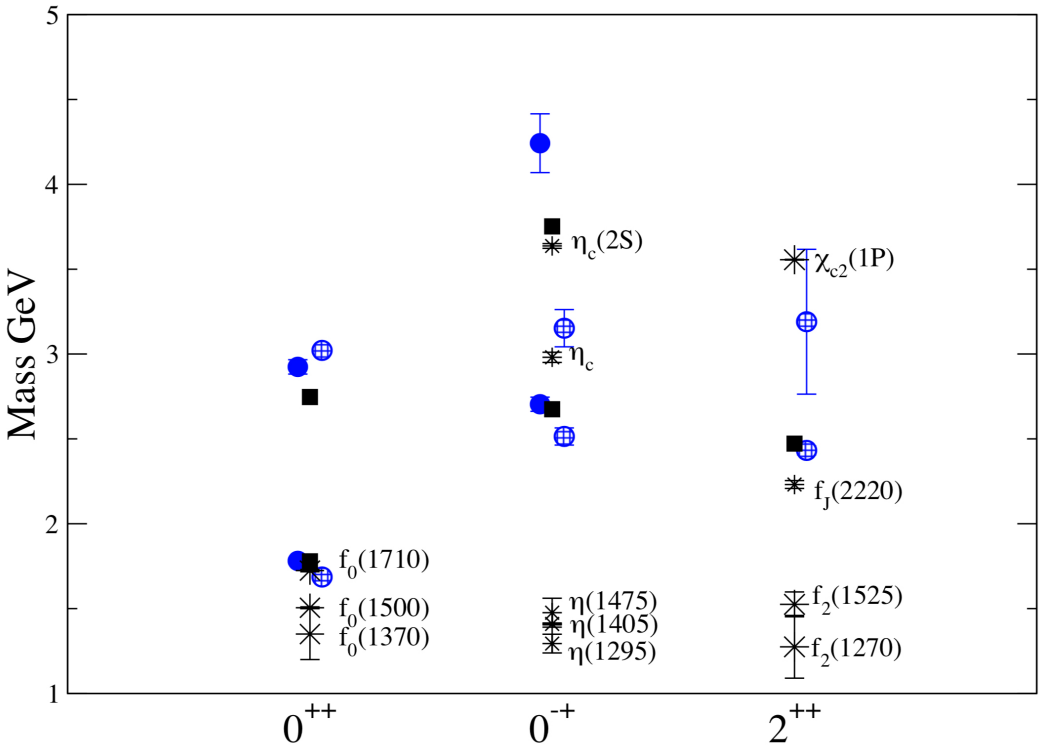

Figure 15.15: Lattice QCD predictions for glueball masses. The open and closed circles are the larger and smaller lattice spacing data of the full QCD calculation of glueball masses of Ref. [125]. Squares are the quenched data for glueball masses of Ref. [25]. The bursts labeled by particle names are experimental states with the appropriate quantum numbers.

agreement with experiment and with quark model expectations.

References

[1] G. 't Hooft, Nucl. Phys. B **72**, 461 (1974).

[2] G. 't Hooft, Nucl. Phys. B **75**, 461 (1974).

[3] E. Witten, Nucl. Phys. B **160**, 57 (1979).

[4] C. Amsler in the Quark Structure of Hadrons, Lecture Notes in Physics **949** (2018), ed. Springer.

[5] H.-Y. Cheng, Physics Letters B **707**, 1, 116 (2012), ISSN 0370-2693, URL https://www.sciencedirect.com/science/article/pii/S0370269311014705.

[6] L. Burakovsky and J. T. Goldman, Nucl. Phys. **A625**, 220 (1997), [hep-ph/9703272].

[7] M.-C. Du and Q. Zhao, Phys. Rev. D **100**, 036005 (2019), URL https://link.aps.org/doi/10.1103/PhysRevD.100.036005.

[8] H.-W. Ke and X.-Q. Li, Phys. Rev. D **99**, 036014 (2019), URL https://link.aps.org/doi/10.1103/PhysRevD.99.036014.

[9] M.-L. Du *et al.*, Phys. Rev. Lett. **126**, 192001 (2021), URL https://link.aps.org/doi/10.1103/PhysRevLett.126.192001.

[10] J. Schwinger, Phys. Rev. **135**, B816 (1964).

[11] H. J. Lipkin and B.-s. Zou, Phys. Rev. D **53**, 6693 (1996).

[12] A. Bramon, R. Escribano and M. D. Scadron, Phys. Lett. **B403**, 339 (1997), [hep-ph/9703313].

[13] A. Aloisio *et al.* (KLOE), Phys. Lett. **B541**, 45 (2002), [hep-ex/0206010].

[14] F. Ambrosino *et al.*, JHEP **07**, 105 (2009), [arXiv:0906.3819].

[15] C. Amsler *et al.* (Crystal Barrel), Phys. Lett. **B294**, 451 (1992).

[16] C. Amsler, Rev. Mod. Phys. **70**, 1293 (1998), [hep-ex/9708025].

[17] N. H. Christ *et al.*, Phys. Rev. Lett. **105**, 241601 (2010), [arXiv:1002.2999].

[18] T. Feldmann, Int. J. Mod. Phys. **A915**, 159 (2000).

[19] C. Amsler and F. E. Close, Phys. Rev. **D53**, 295 (1996), [hep-ph/9507326].

[20] R. L. Jaffe, Phys. Rev. **D15**, 267 (1977).

[21] R. L. Jaffe, Phys. Rev. **D15**, 281 (1977).

[22] Y. Chen *et al.*, Phys. Rev. **D73**, 014516 (2006), [hep-lat/0510074].

[23] S.L. Olsen, Front. Phys. **10**, 121 (2015).

[24] S. L. Olsen, T. Skwarnicki and D. Zieminska, Rev. Mod. Phys. **90**, 1, 015003 (2018), [arXiv:1708.04012].

[25] C. J. Morningstar and M. J. Peardon, Phys. Rev. **D60**, 034509 (1999), [hep-lat/9901004].

[26] W.-J. Lee and D. Weingarten, Phys. Rev. **D61**, 014015 (2000), [hep-lat/9910008].

[27] G. S. Bali *et al.* (UKQCD), Phys. Lett. **B309**, 378 (1993), [hep-lat/9304012].

[28] C. Michael, AIP Conf. Proc. **432**, 1, 657 (1998), [hep-ph/9710502].

[29] F. E. Close and A. Kirk, Eur. Phys. J. **C21**, 531 (2001), [hep-ph/0103173].

[30] W. Ochs, J. Phys. **G40**, 043001 (2013), [arXiv:1301.5183].

[31] F. Brünner and A. Rebhan, Phys. Rev. Lett. **115**, 13, 131601 (2015), [arXiv:1504.05815].

[32] C. Amsler and N. A. Tornqvist, Phys. Rept. **389**, 61 (2004).

[33] N. Isgur and J. E. Paton, Phys. Rev. **D31**, 2910 (1985).

[34] P. Lacock *et al.* (UKQCD), Phys. Lett. **B401**, 308 (1997), [hep-lat/9611011].

[35] M. S. Chanowitz and S. R. Sharpe, Nucl. Phys. **B222**, 211 (1983), [Erratum: Nucl. Phys.B228,588(1983)].

[36] T. Barnes *et al.*, Nucl. Phys. **B224**, 241 (1983).

[37] B. Kopf *et al.* (2020), [arXiv:2008.11566].

[38] R. Aaij *et al.* (LHCb), Phys. Rev. Lett. **115**, 072001 (2015), [arXiv:1507.03414].

[39] R. Aaij *et al.* (LHCb), Phys. Rev. Lett. **122**, 22, 222001 (2019), [arXiv:1904.03947].

[40] J.-J. Wu *et al.*, Phys. Rev. Lett. **105**, 232001 (2010), URL `https://link.aps.org/doi/10.1103/PhysRevLett.105.232001`.

[41] J.-J. Wu, T.-S. H. Lee and B. S. Zou, Phys. Rev. C **85**, 044002 (2012), URL `https://link.aps.org/doi/10.1103/PhysRevC.85.044002`.

[42] Y.-R. Liu *et al.*, Prog. Part. Nucl. Phys. **107**, 237 (2019), [arXiv:1903.11976].

[43] F.E. Close, in *Quarks and Nuclear Forces* (Springer-Verlag, 1982), p. 56.

[44] R.H. Dalitz and L.J. Reinders, in "Hadron Structure as Known from Electromagnetic and Strong Interactions," *Proceedings of the Hadron '77 Conference* (Veda, 1979), p. 11.

[45] E. Klempt and J.-M. Richard, Rev. Mod. Phys. **82**, 1095 (2010), [arXiv:0901.2055].

[46] T. Melde, W. Plessas and B. Sengl, Phys. Rev. **D77**, 114002 (2008), [arXiv:0806.1454].

[47] N. Isgur and G. Karl, Phys. Rev. **D18**, 4187 (1978).

[48] N. Isgur and G. Karl, Phys. Rev. **D19**, 2653 (1979), [Erratum: Phys. Rev.D23,817(1981)].

[49] S. Capstick and W. Roberts, Prog. Part. Nucl. Phys. **45**, S241 (2000), [arXiv:nucl-th/0008028].

[50] S. Capstick and W. Roberts, Phys. Rev. **D58**, 074011 (1998), [arXiv:nucl-th/9804070].

[51] S. Capstick, Phys. Rev. **D46**, 2864 (1992).

[52] R. A. Arndt *et al.*, Phys. Rev. **C74**, 045205 (2006), [arXiv:nucl-th/0605082].

[53] B. Krusche and S. Schadmand, Prog. Part. Nucl. Phys. **51**, 399 (2003), [arXiv:nucl-ex/0306023].

[54] A. V. Anisovich *et al.*, Eur. Phys. J. **A52**, 9, 284 (2016), [arXiv:1604.05704].

[55] E. Gutz *et al.* (CBELSA/TAPS), Eur. Phys. J. **A50**, 74 (2014), [arXiv:1402.4125].

[56] V. Sokhoyan *et al.* (CBELSA/TAPS), Eur. Phys. J. **A51**, 8, 95 (2015), [Erratum: Eur. Phys. J.A51,no.12,187(2015)], [arXiv:1507.02488].

[57] E. Klempt *et al.*, Eur. Phys. J. **A56**, 261 (2020).

[58] J. Yelton *et al.*, Phys. Rev. Lett. **121**, 052003 (2018).

[59] G. Barruca *et al.*, Eur. Phys. J. **A57**, 154 (2021).

[60] G. Barucca *et al.*, Eur. Phys. J **A57**, 4, 154 (2021).

[61] S. Capstick and W. Roberts, Prog. in Part. Nucl. Phys. **45**, 241 (2000).

[62] V. Crede and W. Roberts, Rept. on Prog. in Phys. **76**, 076301 (2013).

[63] M. Ferraris *et al.*, Phys. Lett. **B364**, 231 (1995).

[64] M. M. Giannini and E. Santopinto, Chin. J. Phys. **53**, 020301 (2015), [arXiv:1501.03722].

[65] M. Anselmino *et al.*, Rev. Mod. Phys. **65**, 1199 (1993).

[66] R. Bijker, F. Iachello and A. Leviatan, Annals Phys. **236**, 69 (1994), [arXiv:nucl-th/9402012].

[67] S. Capstick and P. R. Page, Phys. Rev. **C66**, 065204 (2002), [arXiv:nucl-th/0207027].

[68] R. L. Jaffe, D. Pirjol and A. Scardicchio, Phys. Rept. **435**, 157 (2006), [hep-ph/0602010].

[69] R. Slansky, Phys. Rept. **79**, 1 (1981).

[70] M. Karliner and J. L. Rosner, Phys. Rev. **D90**, 9, 094007 (2014), [arXiv:1408.5877].

[71] R. Aaij *et al.* (LHCb), Phys. Rev. Lett. **118**, 18, 182001 (2017), [arXiv:1703.04639].

[72] Y. Yelton *et al.*, Phys. Rev. **D97**, 051102(R) (2018).

[73] R. Aaij *et al.*, Phys. Rev. Lett **124**, 082002 (2020).

[74] R. Aaij *et al.* (LHCb), Phys. Rev. Lett. **119**, 11, 112001 (2017), [arXiv:1707.01621].

[75] M. Mattson *et al.* (SELEX), Phys. Rev. Lett. **89**, 112001 (2002), [hep-ex/0208014].

[76] A. Ocherashvili *et al.* (SELEX), Phys. Lett. **B628**, 18 (2005), [hep-ex/0406033].

[77] R. Aaij *et al.* (LHCb), Sci. China Phys. Mech. Astron. **63**, 2, 221062 (2020), [arXiv:1909.12273].

[78] S. G. S.J. Brodsky and S. Koshkarev, Eur. Phys. J. **C78**, 483 (2018).

[79] R. Aaij *et al.* (LHCb), JHEP **05**, 030 (2017), [arXiv:1701.07873].

[80] L. Schachinger *et al.*, Phys. Rev. Lett. **41**, 1348 (1978).

[81] A. Morelos Pineda *et al.* (E761), Phys. Rev. Lett. **71**, 3417 (1993).

[82] D. W. Hertzog *et al.*, Phys. Rev. D **37**, 1142 (1988).
[83] N. B. Wallace *et al.*, Phys. Rev. Lett. **74**, 3732 (1995).
[84] A. Bosshard *et al.*, Phys. Rev. D **44**, 1962 (1991).
[85] M. Kotulla *et al.*, Phys. Rev. Lett **27**, 272001 (2002).
[86] S. Schumann *et al.*, Eur. Phys. J. **A43**, 269 (2010).
[87] A. De Rujula, H. Georgi and S. L. Glashow, Phys. Rev. **D12**, 147 (1975).
[88] W. H. Blask *et al.*, Z. Phys. **A337**, 327 (1990).
[89] U. Loring *et al.*, Eur. Phys. J. **A10**, 309 (2001), [hep-ph/0103287].
[90] L. Ya. Glozman and D. O. Riska, Phys. Rept. **268**, 263 (1996), [hep-ph/9505422].
[91] T. DeGrand and E. T. Neil, Phys. Rev. D **101**, 3, 034504 (2020), [arXiv:1910.08561].
[92] C. Aubin *et al.*, Phys. Rev. **D70**, 094505 (2004), [hep-lat/0402030].
[93] A. Bazavov *et al.* (MILC), Rev. Mod. Phys. **82**, 1349 (2010), [arXiv:0903.3598].
[94] S. Aoki *et al.* (PACS-CS), Phys. Rev. **D79**, 034503 (2009), [arXiv:0807.1661].
[95] S. Durr *et al.*, Science **322**, 1224 (2008), [arXiv:0906.3599].
[96] W. Bietenholz *et al.*, Phys. Rev. **D84**, 054509 (2011), [arXiv:1102.5300].
[97] C. Alexandrou *et al.*, Phys. Rev. **D90**, 7, 074501 (2014), [arXiv:1406.4310].
[98] J. J. Dudek *et al.*, Phys. Rev. **D83**, 111502 (2011), [arXiv:1102.4299].
[99] E. B. Gregory *et al.* (UKQCD), Phys. Rev. **D86**, 014504 (2012), [arXiv:1112.4384].
[100] C. Michael, K. Ottnad and C. Urbach (ETM), Phys. Rev. Lett. **111**, 18, 181602 (2013), [arXiv:1310.1207].
[101] C. Bernard *et al.* (Fermilab Lattice, MILC), Phys. Rev. **D83**, 034503 (2011), [arXiv:1003.1937].
[102] E. B. Gregory *et al.*, Phys. Rev. **D83**, 014506 (2011), [arXiv:1010.3848].
[103] R. J. Dowdall *et al.*, Phys. Rev. **D86**, 094510 (2012), [arXiv:1207.5149].
[104] D. Mohler and R. M. Woloshyn, Phys. Rev. **D84**, 054505 (2011), [arXiv:1103.5506].
[105] A. S. Kronfeld, Ann. Rev. Nucl. Part. Sci. **62**, 265 (2012), [arXiv:1203.1204].
[106] K. Ottnad, C. Urbach and F. Zimmermann (OTM), Nucl. Phys. **B896**, 470 (2015), [arXiv:1501.02645].
[107] C. DeTar *et al.* (Fermilab Lattice, MILC), Phys. Rev. D **99**, 3, 034509 (2019), [arXiv:1810.09983].
[108] L. Liu *et al.*, Phys. Rev. **D81**, 094505 (2010), [arXiv:0909.3294].
[109] R. A. Briceno, H.-W. Lin and D. R. Bolton, Phys. Rev. **D86**, 094504 (2012), [arXiv:1207.3536].
[110] Y. Namekawa *et al.* (PACS-CS), Phys. Rev. **D87**, 9, 094512 (2013), [arXiv:1301.4743].
[111] M. Padmanath *et al.*, Phys. Rev. **D90**, 7, 074504 (2014), [arXiv:1307.7022].
[112] Z. S. Brown *et al.*, Phys. Rev. **D90**, 9, 094507 (2014), [arXiv:1409.0497].
[113] P. Pérez-Rubio, S. Collins and G. S. Bali, Phys. Rev. **D92**, 3, 034504 (2015), [arXiv:1503.08440].
[114] C. Alexandrou and C. Kallidonis, Phys. Rev. **D96**, 3, 034511 (2017), [arXiv:1704.02647].
[115] S. Meinel, private comunication .

[116] R. A. Briceno, J. J. Dudek and R. D. Young, Rev. Mod. Phys. **90**, 2, 025001 (2018), [arXiv:1706.06223].

[117] J. Bulava *et al.*, Nucl. Phys. **B910**, 842 (2016), [arXiv:1604.05593].

[118] R. A. Briceno *et al.*, Phys. Rev. Lett. **118**, 2, 022002 (2017), [arXiv:1607.05900].

[119] D. Guo *et al.*, Phys. Rev. D **98**, 1, 014507 (2018), [arXiv:1803.02897].

[120] C. W. Andersen *et al.*, Phys. Rev. **D97**, 1, 014506 (2018), [arXiv:1710.01557].

[121] J. J. Dudek *et al.* (Hadron Spectrum), Phys. Rev. **D88**, 9, 094505 (2013), [arXiv:1309.2608].

[122] R. G. Edwards *et al.*, Phys. Rev. **D84**, 074508 (2011), [arXiv:1104.5152].

[123] A. J. Woss *et al.* (Hadron Spectrum), Phys. Rev. D **103**, 5, 054502 (2021), [arXiv:2009.10034].

[124] C. T. Johnson and J. J. Dudek (Hadron Spectrum), Phys. Rev. D **103**, 7, 074502 (2021), [arXiv:2012.00518].

[125] C. M. Richards *et al.* (UKQCD), Phys. Rev. **D82**, 034501 (2010), [arXiv:1005.2473].

[126] E. Gregory *et al.*, JHEP **10**, 170 (2012), [arXiv:1208.1858].

[127] R. F. Lebed, R. E. Mitchell and E. S. Swanson, Prog. Part. Nucl. Phys. **93**, 143 (2017), [arXiv:1610.04528].

[128] E. J. Eichten and C. Quigg, Phys. Rev. Lett. **119**, 20, 202002 (2017), [arXiv:1707.09575].

[129] L. Leskovec *et al.*, Phys. Rev. D **100**, 1, 014503 (2019), [arXiv:1904.04197].

[130] A. Francis *et al.*, Phys. Rev. Lett. **118**, 14, 142001 (2017), [arXiv:1607.05214].

[131] M. Karliner and J. L. Rosner, Phys. Rev. Lett. **119**, 20, 202001 (2017), [arXiv:1707.07666].

[132] M. Karliner and J. L. Rosner (2019), [arXiv:1906.07799].

[133] S. Aoki *et al.* (Flavour Lattice Averaging Group), Eur. Phys. J. C **80**, 2, 113 (2020), [arXiv:1902.08191].

[134] S. Borsanyi *et al.*, Science **347**, 1452 (2015), [arXiv:1406.4088].

[135] G. M. de Divitiis *et al.* (RM123), Phys. Rev. D **87**, 11, 114505 (2013), [arXiv:1303.4896].

[136] D. Giusti *et al.*, Phys. Rev. **D95**, 11, 114504 (2017), [arXiv:1704.06561].

[137] S. Basak *et al.* (MILC), Phys. Rev. D **99**, 3, 034503 (2019), [arXiv:1807.05556].

[138] A. Parreno *et al.*, Phys. Rev. D **95**, 11, 114513 (2017), [arXiv:1609.03985].